TITLE

TRPA1 is a source of calcium-mediated cardiac mechano-arrhythmogenesis

AUTHORS

Breanne A. Cameron[1]

Matthew R. Stoyek[1]

Jessi J. Bak[1]

Michael S. Connolly[1]

Joachim Greiner[2]

Rémi Peyronnet[2]

Peter Kohl[2,3]

*T Alexander Quinn[1,4]

AFFILIATIONS

[1]Department of Physiology and Biophysics, Dalhousie University, Halifax, Canada

[2]Institute for Experimental Cardiovascular Medicine, University Heart Center Freiburg · Bad Krozingen and Faculty of Medicine, University of Freiburg, Freiburg, Germany

[3]Faculty of Engineering, University of Freiburg, Freiburg, Germany

[4]School of Biomedical Engineering, Dalhousie University, Halifax, Canada

SUMMARY PARAGRAPH

Maintenance of cardiac function involves an important intrinsic regulatory loop, in which electrical excitation causes the heart to mechanically contract,[1] and the cardiac mechanical state directly affects its electrical activity.[2] In diseases that affect myocardial mechanical properties and function, it is thought that this feedback of mechanics to electrics may contribute to arrhythmias ('mechano-arrhythmogenesis').[3] However, the molecular identity of the specific factor(s) underlying mechano-arrhythmogenesis are unknown.[4] We show in rabbit ventricular myocytes that mechano-sensitive[5-11] transient receptor potential kinase ankyrin 1 (TRPA1) channels[12] are a source of cardiac mechano-arrhythmogenesis through a calcium (Ca^{2+})-mediated mechanism. Using a cell-level approach involving rapid stretch of single ventricular myocytes, we found that increased TRPA1 activity results in stretch-induced arrhythmias, with trans-sarcolemmal depolarising arrhythmic triggers mediated by increased diastolic levels of cytosolic Ca^{2+} and sustained arrhythmic activity driven by cytosolic Ca^{2+} oscillations. This mechano-arrhythmogenesis increased with application of a microtubule stabilising agent and was prevented by pharmacological TRPA1 channel block or buffering of cytosolic Ca^{2+}. Our results demonstrate that TRPA1 channels can act as a trigger for stretch-induced excitation and create a substrate for sustained arrhythmias. TRPA1 channels may thus represent a novel anti-arrhythmic target in cardiac diseases in which their activity is augmented.[13-17]

MAIN TEXT

Feedback is an essential element of biological function and fundamental to the control and adaptation of physiological activity. A prime example is seen in the heart, which is an electro-mechanical pump wherein electrical excitation of cardiac myocytes causes their contraction through a feedforward mechanism involving triggered release of calcium (Ca^{2+}) from intracellular stores, known as 'excitation-contraction coupling'.[1] Feedback in this system involves the influence of the mechanical state of cardiac myocytes on their electrical activity, by a process termed 'mechano-electric coupling'.[2] In healthy conditions, this feedback is important for fine tuning normal cardiac function.[18] In diseases involving haemodynamic overload and altered myocardial mechanical properties or function¸ mechano-electric coupling may instead contribute to cardiac arrhythmias through arrhythmogenic electrophysiological effects ('mechano-arrhythmogenesis').[3] While the influence of mechano-electric coupling on cardiac electrophysiology is well established,[2] the molecular identity of the specific factor(s) involved, especially those underlying mechano-arrhythmogenesis, are still being explored.[4]

Here we utilised a cell-level approach for investigating mechanisms of mechano-arrhythmogenesis, which allowed for the control of single cell mechanical load with a carbon fibre-based system.[19] This was combined with simultaneous fluorescence imaging of trans-membrane voltage and cytosolic Ca^{2+}, video-based measurement of sarcomere dynamics, and pharmacological interrogation of mechanisms suspected to be mediating arrhythmias that occurred upon cell stretch.

Recent results from rabbit isolated heart studies suggest that ventricular mechano-arrhythmogenesis in acute regional ischaemia (as occurs with occlusion of a coronary artery) is caused by a mechano-sensitive Ca^{2+}-mediated mechanism. This dependence on Ca^{2+} may be

facilitated by a disruption in what we are calling 'repolarisation-relaxation coupling' (RRC), a process that describes the interaction between recovery of membrane potential and intracellular Ca^{2+} to diastolic levels, which ultimately facilitates relaxation. In ischaemia, activation of ATP-sensitive potassium (K_{ATP}) channels increase the repolarising drive, resulting in a pathological dissociation of RRC reflected by a larger shortening of action potential than Ca^{2+}-transient duration (APD and CaTD, respectively).[20] As a result of disturbed RRC, a potentially vulnerable period (VP_{RRC}) for Ca^{2+}-mediated arrhythmias forms during late repolarisation, as cytosolic Ca^{2+} remains elevated in progressively re-excitable tissue[21,22] (a similar VP_{RRC} has been shown to occur during beta-adrenergic stimulation in failing human hearts[23]). In the present study, we utilised our single cell system to investigate the specific influence of a K_{ATP} channel activation-induced VP_{RRC} on the susceptibility of left ventricular myocytes to stretch-induced excitation and sustained arrhythmic activity, and to determine mechanisms underlying ventricular mechano-arrhythmogenesis.

K_{ATP} channels were activated by application of pinacidil (50 μM, continuous superfusion), a well-established agonist of sulfonylurea receptor (SUR)2A/K_{ir}6.2 in cardiac and skeletal muscle.[24] To assess effects of K_{ATP} channel activation on the relative recovery-time of voltage and Ca^{2+} and on the size of the resultant VP_{RRC}, we used a single-excitation/dual-emission fluorescence imaging approach[25] (with di-4-ANBDQPQ and Fluo-5F, AM, which has a relatively high K_d value [~2.3 μM], limiting its buffering of Ca^{2+} and artefactual increase in measured Ca^{2+} transient duration). This approach allowed us to simultaneously record action potentials and Ca^{2+} transients in electrically-paced rabbit left ventricular myocytes under carbon fibre control (Fig. 1a). With pinacidil exposure, both APD and CaTD decreased (Fig. 1b, c). However, the decrease of APD was significantly greater than that of CaTD, resulting in the formation of a cellular VP_{RRC} (defined

as the period during which a myocyte starts to become re-excitable while cytosolic Ca^{2+} remains elevated, calculated as the difference between CaTD at 80% recovery and APD at 50% recovery of diastolic levels; Fig. 1b, d). This response mimics the behaviour previously observed in whole hearts during acute ischaemia[20,21] (as well as with hypoxia alone[22]). After 5 min of pinacidil exposure, there were no further significant alterations in APD, CaTD, or the VP_{RRC} (Fig. 1c, d).

Having shown that we were able to generate a cellular VP_{RRC} by K_{ATP} activation, we sought to determine whether stretch specifically during the VP_{RRC} resulted in an increase in mechano-arrhythmogenesis. Rapid, transient stretch – as occurs in ischaemically weakened myocardium in the whole heart[26] – was applied with carbon fibres adhered to either end of single cells and under piezo-electric translator control (Fig. 2a). Stretches (with a range of percent sarcomere stretch, stretched sarcomere length, and maximal applied stress) were timed from the pacing stimulus to occur either during the VP_{RRC} or in diastole (Fig. 2b, c). The parameters of these stretches were assessed within a single cell exposed to physiologic or pinacidil-containing solution (Extended Data Fig. 1). Stretch resulted in a variety of changes in rhythm (revealed by tracking sarcomere length), including premature contractions (defined as 1 or 2 contractions out of sync with ongoing electrical stimulation; Fig. 2d and Supplementary Video 1) and a variety of other arrhythmic responses (*i.e.*, refractoriness resulting in a single [Fig. 2e] or multiple [Fig. 2f, Supplementary Video 2] missed beat(s), or sustained activity that either spontaneously resolved [Fig. 2g] or was terminated by application of an additional stretch [Fig. 2h, Supplementary Video 3]). While it was found that the incidence of arrhythmic activity was greater in pinacidil-treated cells than in control, it was not significantly different for stretch applied during the VP_{RRC} compared to stretch in diastole, suggesting that the pinacidil-treated cells were generally more prone to mechano-arrhythmogenesis (Fig. 3a and Extended Data Fig. 2).

As previous work in the whole heart has shown that the magnitude of tissue deformation is a key determinant of mechano-arrhythmogenesis,[27] we also assessed the effect of stretch characteristics on arrhythmia incidence. Increasing the piezo-electric translator displacement from 20 to 40 μm resulted in an increase from pre-stretch values in the percent sarcomere stretch, stretched sarcomere length, and maximal applied stress, which scaled with piezo-electric translator displacement (Extended Data Fig. 1). These increases in applied load raised the incidence of stretch-induced arrhythmias in pinacidil-treated cells (arrhythmia incidence remained low in control cells; Extended Data Fig. 3), indicating that the increase in mechano-arrhythmogenesis that occurs with pinacidil treatment scales with the degree of cell stretch.

To assess whether arrhythmias could be the result of stretch-induced cellular damage, contractile function was assessed before and after stretch at each magnitude. In both control and pinacidil-treated cells, diastolic sarcomere length and the maximal rate and percent of sarcomere shortening during contraction were not significantly different before and after successive stretches with increased piezo-electric translator displacement (Extended Data Fig. 4). These parameters were also not significantly different before stretch and after return to steady state following sustained arrhythmic activity (Extended Data Fig. 5), suggesting that cellular damage does not explain the observed arrhythmias.

Since we found that pinacidil increased the incidence of stretch-induced arrhythmias, which was not restricted to stretch in the VP_{RRC}, we sought to determine the source of the overall increase in mechano-arrhythmogenesis. K_{ATP} channels are mechano-sensitive, with their current being increased by stretch when active,[28] so it is tempting to think they may have been involved. However, as K_{ATP} channels are highly selective for potassium, they have a reversal potential of ~-90 mV and conduct an outward potassium current over the working range of membrane potentials

of ventricular myocytes. As a result, their activation in ventricular myocytes will always contribute to repolarisation, so they cannot account for the stretch-induced excitation seen in this and other studies (in fact, they would be expected to oppose depolarisation). Alternatively, while pinacidil is generally thought of as a specific activator of K_{ATP} channels, it has also been shown to increase the activity of transient receptor potential kinase ankyrin 1 (TRPA1) channels in HEK293 cells,[29] resulting in a depolarising trans-membrane influx. Importantly, TRPA1 channels: (i) are inherently mechano-sensitive[5] and contribute to mechanically-evoked action potentials[6] and currents in sensory neurons,[7,8] astrocytes,[9] and vertebrate hair cells;[10] (ii) have been shown to be functionally expressed in ventricular myocytes of mice[30] (although others have found conflicting results[31]) and to drive changes in rhythm in response to mechanical stimulation in the *Drosophila* heart;[11] and (iii) are important in a range of cardiovascular functions and pathologies.[13] We hypothesised that if TRPA1 channels are functionally expressed in rabbit ventricular myocytes, then they could contribute to the increase in mechano-arrhythmogenesis seen in our experiments.

To assess the presence and function of TRPA1 channels in the rabbit left ventricle, we first measured TRPA1 protein expression in left ventricular free wall tissue by Western blotting, which revealed robust expression (Extended Data Fig. 6a). Next, functional expression of TRPA1 channels in left ventricular myocytes was evaluated by measuring ion channel activity in cell-attached patches during application of the TRPA1 channel-specific agonist allyl isothiocyanate (AITC; 50 μM),[32] which has been shown to activate TRPA1 channels in human adult ventricular cardiac fibroblasts,[33] amongst other cell types. It was found that AITC exposure caused an increase in total current, while there was no change in time-matched control cells (Extended Data Fig. 6b, c).

The above results suggest that mechano-sensitive TRPA1 channels are functionally expressed in rabbit ventricular myocytes and that their activation may account for the increase in mechano-arrhythmogenesis seen in our experiments. Therefore, we further explored their potential involvement in mechano-arrhythmogenesis by applying to pinacidil-treated cells either a non-specific blocker of cation non-selective mechano-sensitive channels (streptomycin;[34] 50 μM, 5 min superfusion) or a specific TRPA1 channel blocker, which has been shown to inhibit TRPA1 current and mechanically-induced excitation in sensory neurons[6-8] (HC-030031;[35] 10 μM, 30 min incubation). Both streptomycin and HC-030031 reduced the incidence of arrhythmias with stretch in the VP_{RRC} and during diastole (Fig. 3a; arrhythmia incidence remained low in control cells, Extended Data Fig. 2). Importantly, streptomycin and HC-030031 appeared to have no other functional effects, as diastolic and contractile function were preserved during their application in control cells (Extended Data Fig. 7).

Next, as TRPA1 channels preferentially pass Ca^{2+} into cells (~5× that of sodium),[36] we assessed whether Ca^{2+} contributes to mechano-arrhythmogenesis by buffering cytosolic Ca^{2+} with BAPTA-AM (1 μM, 20 min incubation), which has been shown previously in ventricular myocytes to prevent stretch-induced changes in cardiac electrophysiology driven by changes in intracellular Ca^{2+}.[37] BAPTA also reduced arrhythmia incidence both in the VPRRC and during diastole in pinacidil-treated cells, suggesting that Ca^{2+} is indeed playing a role (Fig. 3a). To explore whether there may have also been a contribution of stretch-induced intracellular Ca^{2+} release from the sarcoplasmic reticulum to the observed arrhythmias, ryanodine receptors were stabilised in their closed state with dantrolene (1 μM, 5 min of superfusion, which does not affect Ca^{2+}-induced Ca^{2+} release or contraction[38]). Yet, dantrolene had no effect on arrythmia incidence. In control cells, the incidence of stretch-induced arrhythmias remained low with BAPTA or dantrolene exposure

(Extended Data Fig. 2), and there was no effect on diastolic sarcomere length or maximal rate of systolic sarcomere shortening. There was, however, a slight decrease in the percent of systolic sarcomere shortening, presumably due to binding of Ca^{2+} by BAPTA (Extended Data Fig. 7).

We then sought to specifically explore whether TRPA1 channels are a source of mechano-arrhythmogenesis. Control cells were exposed to AITC (10 µM, 5 min superfusion), which enhances the response of TRPA1 channels to mechanical stimulation,[8] and subjected to diastolic stretch (VP_{RRC} stretches were not applied to these cells, as simultaneous disruption of RRC with pinacidil was absent). AITC caused an increase in arrythmia incidence in diastole compared to both control and pinacidil-treated cells (Fig. 3b), which was prevented by co-application of the TRPA1-blocker HC-030031 (Fig. 3b). Finally, as in pinacidil-treated cells, BAPTA also prevented an increase in the incidence of stretch-induced arrhythmias during AITC treatment (Fig. 3b), further supporting a role of Ca^{2+} in the observed increase in mechano-arrhythmogenesis.

While the above findings strongly suggest a role of TRPA1 channels in stretch-induced arrhythmogenesis, we did not find an increase in TRPA1 current in our patch-clamp experiments when the cell membrane was stretched by negative pipette pressure. However, as there is a large body of evidence demonstrating that interactions between TRP channels and microtubules are important for TRP channel function,[39] we hypothesised that microtubule-mediated mechano-transduction during axial cell stretch may be necessary for a mechanically-induced response (which would not have been engaged during membrane stretch by patch pipette). To test for the importance of microtubules in mechano-arrhythmogenesis, cells were exposed to paclitaxel (10 µM, 90 min incubation) to increase polymerisation and stabilisation of microtubules,[40] which has been shown to increase the probability of stretch-induced arrhythmias in the isolated rabbit heart.[41] We showed that paclitaxel did indeed increase the microtubule density of our ventricular myocytes

using immunofluorescence imaging (Extended Data Fig. 8), and that paclitaxel treatment resulted in an increase in the incidence of arrhythmias with stretch in diastole (Fig. 3b). Interestingly, this arrhythmogenic effect appears to involve interactions with TRPA1 channels, as their block with HC-030031 prevented the increase in mechano-arrhythmogenesis during paclitaxel treatment (Fig. 3b).

Our results to this point suggested that an inward current passing through mechano-sensitive TRPA1 channels acts as a trigger for stretch-induced premature contractions, however the source of the sustained arrhythmic activity induced by stretch remained unclear. As TRPA1 channel activity has been shown to cause an increase in diastolic Ca^{2+} concentration in ventricular myocytes,[42] which can create an arrhythmogenic substrate,[43] contribute to sarcoplasmic reticulum Ca^{2+} release, and further activate TRPA1 channels,[44] we hypothesised that TRPA1-mediated effects on cytosolic Ca^{2+} may account for the increase in sustained arrhythmic activity observed in our experiments. We measured free cytosolic Ca^{2+} concentration ($[Ca^{2+}]_i$) with a ratiometric fluorescence imaging technique (using Fura Red, AM; K_d = 400 nM), which showed that both pinacidil and AITC increased $[Ca^{2+}]_i$ in diastole (Fig. 3c). However, despite an anti-arrhythmic effect in both AITC and pinacidil-treated cells, blocking TRPA1 channels with HC-030031 reduced the increase in diastolic $[Ca^{2+}]_i$ only for AITC treatment (Fig. 3c), suggesting that the increase in diastolic $[Ca^{2+}]_i$ with AITC and pinacidil may be occurring in part through different mechanisms. As chelating cytosolic $[Ca^{2+}]_i$ with BAPTA for both treatments was also anti-arrhythmic, this suggested that increased cytosolic $[Ca^{2+}]_i$ may be necessary, but not sufficient for the increase in mechano-arrhythmogenesis (unfortunately, we could not measure the effects of BAPTA on cytosolic $[Ca^{2+}]_i$, as the combined Ca^{2+} buffering by BAPTA and Fura Red greatly affected cell contraction). Explicit evidence for a direct role of Ca^{2+} in the sustained arrhythmic

activity came from dual voltage-Ca^{2+} fluorescence imaging, which revealed an increase in cytosolic $[Ca^{2+}]_i$, along with Ca^{2+} oscillations that precede oscillations in voltage during sustained arrhythmias, indicating that Ca^{2+} was driving the aberrant behaviour (Fig. 4a, Supplementary Video 4). It is worth noting, here, that changes in repolarisation can also destabilise the electrical activity of ventricular myocytes. Thus, in the pinacidil-treated cells, a stretch-induced increase in K_{ATP} channel current may also have directly contributed to the sustained arrhythmias and may account for the temporary refractoriness caused by stretch in some cells.[28]

Finally, with an increase in cytosolic $[Ca^{2+}]_i$, there is the possibility that a change in cellular mechanics may also contribute to mechano-arrhythmogenesis by enhancing mechano-transduction or altering the characteristics of stretch. However, there was no effect of pinacidil on cell stiffness or elastance (measured as the slopes of end-diastolic and end-systolic stress-length relationship in contracting cells; Extended Data Fig. 9), or the percent sarcomere stretch, stretched sarcomere length, or maximal applied stress during stretch (Extended Data Fig. 1), suggesting that changes in cellular mechanics were not a major contributor to observed effects (note: there was a shift in the stiffness and elastance curves to the right in pinacidil-treated cells, which may relate to a reduced myofilament Ca^{2+} affinity through TRPA1-induced phosphorylation of troponin I;[42] Extended Data Fig. 9). Further, in a subset of pinacidil-treated cells for which two consecutive diastolic stretches of the same magnitude first did, and then did not, result in an arrhythmia, the characteristics of each stretch were similar (Extended Data Fig. 10), suggesting that stretch characteristics were not the primary determinant of the occurrence of stretch-induced arrhythmias.

Taken together, our results suggest that TRPA1 channels are a source of Ca^{2+}-mediated ventricular mechano-arrhythmogenesis. Figure 4b summarises our results and presents a working model of the role that TRPA1 channels play in triggering stretch-induced excitation (through a

depolarising trans-sarcolemmal influx) and in creating a substrate for sustained arrhythmic activity (through increasing $[Ca^{2+}]_i$). TRPA1 channels are mechano-sensitive and allow trans-sarcolemmal cation influx with stretch that will depolarise cell membrane potential. At the same time, the associated increase in cytosolic $[Ca^{2+}]_i$ will further depolarise membrane potential *via* electrogenic forward-mode sodium-Ca^{2+} exchanger current, while also creating an arrhythmia sustaining substrate.[43] If the combined depolarisation is sufficiently large, it will cause excitation and premature contraction of the cell. Further, TRPA1 channel activity itself is directly modulated by cytosolic $[Ca^{2+}]_i$ in a bimodal fashion.[45] As a result, an increase in $[Ca^{2+}]_i$ will potentiate TRPA1 channel activity, thus further increasing its contribution to mechano-arrhythmogenesis, but at a certain level, cytosolic $[Ca^{2+}]_i$ will instead inactivate some channels, thus limiting the degree of Ca^{2+} overload and preventing lethal cell damage.[45] In our experiments, exposure to AITC caused direct activation of TRPA1 channels and subsequent diastolic Ca^{2+} loading, while pinacidil either directly activated TRPA1 channels, or did so indirectly *via* an increase in cytosolic $[Ca^{2+}]_i$. In both cases, TRPA1 activation would lead to an enhanced depolarising current with stretch, in the presence of increased cytosolic $[Ca^{2+}]_i$ levels (further driving depolarisation and acting as a substrate for sustained arrhythmias). In this way, TRPA1 channels act as the central player in a feed-forward loop that increases Ca^{2+}-dependent mechano-arrhythmogenesis. The role of TRPA1 channels in the stretch-induced arrhythmias observed in our model is supported by the reduction in arrhythmia incidence with specific block of TRPA1 channels by HC-030031 or non-specific block of mechano-sensitive channels by streptomycin. Interestingly, the contribution of TRPA1 channels to mechano-arrhythmogenesis appears to depend on microtubules, as an increase in their polymerisation and stability with paclitaxel increased stretch-induced arrythmia incidence, which was prevented by HC-030031. Finally, the contribution of trans-sarcolemmal Ca^{2+} influx as an

arrhythmogenic trigger and Ca^{2+} overload as an arrhythmia sustaining substrate during TRPA1 channel activation is supported by the reduction in stretch-induced arrhythmias with their block by HC-030031 and buffering of Ca^{2+} by BAPTA.

These findings have potentially important implications for anti-arrhythmic treatment in cardiac diseases with augmented TRPA1 channel expression or activity.[13] This is especially true for diseases in which additional factors activate TRPA1 channels (*e.g.*, oxidative stress),[46] as the response of TRPA1 channels to mechanical stimulation is enhanced by an increase in their baseline activity.[8] For instance, acute myocardial ischaemia is associated with TRPA1-mediated myocardial damage[14] and lethal ventricular arrhythmias that are thought to involve contributions of altered tissue mechanics, intracellular Ca^{2+} handling, and oxidative stress.[26] Thus, targeting TRPA1 channels in that setting could help to prevent multiple detrimental outcomes.[15] This may also be true in chronic pathologies associated with changes in cardiac mechanics, intracellular Ca^{2+}, oxidative stress, and other TRPA1 modulating factors,[12] in which lethal arrhythmias occur, such as ventricular pressure overload (TRPA1 inhibition has been shown to reduce hypertrophy and fibrosis in that setting[16]), making TRPA1 channels a novel anti-arrhythmic target with exciting therapeutic potential.[17]

MAIN REFERENCES

1. Bers, D. M. Cardiac excitation-contraction coupling. *Nature*. **415**, 198-205 (2002).
2. Quinn, T. A. & Kohl, P. Cardiac mechano-electric coupling: acute effects of mechanical stimulation on heart rate and rhythm. *Physiol. Rev.* **101**, 37-92 (2021).
3. Quinn, T. A. The importance of non-uniformities in mechano-electric coupling for ventricular arrhythmias. *J. Interv. Card. Electrophysiol.* **39**, 25-35 (2014).
4. Peyronnet, R., Nerbonne, J. M. & Kohl, P. Cardiac mechano-gated ion channels and arrhythmias. *Circ. Res*. **118**, 311-29 (2016).
5. Moparthi, L. & Zygmunt P. M. Human TRPA1 is an inherently mechanosensitive bilayer-gated ion channel. *Cell Calcium* **91**, 102255 (2020).
6. Kerstein, P.C., del Camino, D., Moran, M. M. & Stucky, C. L. Pharmacological blockade of TRPA1 inhibits mechanical firing in nociceptors. *Mol. Pain* **5**, 19 (2009).
7. Vilceanu, D. & Stukcy, C. L. TRPA1 mediates mechanical currents in the plasma membrane of mouse sensory neurons. *PLoS One* **5**, e12177 (2010).
8. Brierly S. M., *et al*. TRPA1 contributes to specific mechanically activated currents and sensory neuron mechanical hypersensitivity. *J. Physiol*. **589**, 3575-93 (2011).
9. Oh, S-J. *et al*. Ultrasonic neuromodulation via astrocytic TRPA1. *Curr. Biol*. **29**, 3386-401 (2019).
10. Corey, D. P., *et al*. TRPA1 is a candidate for the mechanosensitive transduction channel of vertebrate hair cells. *Nature* **432**, 723-30 (2004).
11. Sénatore S., Reddy, V. R., Sémériva, M., Perrin, L. & Lalevée, N. Response to mechanical stress is mediated by the TRPA channel painless in the *Drosophila* heart. *PLoS Genet.* **6**, e1001088 (2010).

12. Meents, J. E., Ciotu, C. I. & Fischer, M. J. M. TRPA1: a molecular view. *J. Neurophysiol.* **121**, 427-443 (2019).

13. Wang, Z. *et al*. The TRPA1 channel in the cardiovascular system: promising features and challenges. *Front*. *Pharmacol.* **10**, 1253 (2019).

14. Conklin, D. J., *et al*. TRPA1 channel contributes to myocardial ischemia-reperfusion injury. *Am. J. Physiol. Heart. Circ. Physiol.* **316**, H889-99 (2019).

15. Li, R., Liu, R., Yan, F., Zhuang, X., Shi, H. & Gao, X. Inhibition of TRPA1 promotes cardiac repair in mice after myocardial infarction. *J. Cardiovasc. Pharmacol.* **75**, 240-9 (2020).

16. Wang, Z. *et al*. TRPA1 inhibition ameliorates pressure overload-induced cardiac hypertrophy and fibrosis in mice. *E. Bio. Medicine* **36**, 54-62 (2018).

17. Moran, M. M. TRP channels as potential drug targets. *Annu. Rev. Pharmacol. Toxicol.* **58**, 309-30 (2018).

18. Quinn, T. A. Cardiac mechano-electric coupling: a role in regulating normal function of the heart? *Cardiovasc. Res*. **108**, 1-3 (2015).

19. Iribe, G., Helmes, M. & Kohl, P. Force-length relations in isolated intact cardiomyocytes subjected to dynamic changes in mechanical load. *Am. J. Physiol. Circ. Physiol.* **292**, H1487-97 (2007).

20. Baumeister, P., *et al.* Mechanically-induced ventricular arrhythmias during acute regional ischemia. *J. Mol. Cell. Cardiol*. **124,** 87-8 (2018).

21. Tang, L., Joung, B., Ogawa, M., Chen, P. S. & Lin S. F. Intracellular calcium dynamics, shortened action potential duration, and late-phase 3 early afterdepolarization in Langendorff-perfused rabbit ventricles. *J. Cardiovasc. Electrophysiol.* **12**, 1364-71 (2012).

22. Takahashi, M., Yokoshiki, H., Mitsuyama, H., Watanabe, M., Temma, T., Kamada, R., Hagiwara, H., Takahashi, Y., Anzai, T. SK channel blockade prevents hypoxia-induced ventricular arrhythmias through inhibition of Ca2+/voltage uncoupling in hypertrophied hearts. *Am. J. Physiol. Heart. Circ. Physiol*. **320**, H1456-69 (2021).

23. Lang, D., *et al*. Arrhythmogenic remodeling of β_2 versus β_1 adrenergic signaling in the human failing heart. *Circ. Arrhythm. Electrophysiol.* **8**, 409-19 (2015).

24. Fujita, A. & Kurachi, Y. Molecular aspects of ATP-sensitive K^+ channels in the cardiovascular system and K^+ channel openers. *Pharmacol. Ther.* **85**, 39-53 (2000).

25. Quinn, T. A., *et al*. Electrotonic coupling of excitable and nonexcitable cells in the heart revealed by optogenetics. *Proc. Natl. Acad. Sci. U S A.* **113**:14852-7 (2016).

26. Carmeliet, E. Cardiac ionic currents and acute ischemia: from channels to arrhythmias. *Physiol. Rev.* **79**, 917-87 (1999).

27. Quinn, T. A., Jin, H., Lee, P. & Kohl, P. Mechanically induced ectopy via stretch-activated cation-nonselective channels is caused by local tissue deformation and results in ventricular fibrillation if triggered on the repolarization wave edge (*Commotio cordis*). *Circ. Arrhythm. Electrophysiol*. **10**, e004777 (2017).

28. Van Wagoner, D. R. Mechanosensitive gating of atrial ATP-sensitive potassium channels. *Circ. Res.* **72**: 973–83 (1993).

29. Ma, L. H., *et al*. Pinacidil, a K_{ATP} channel opener, identified as a novel agonist for TRPA1. *Chinese Sci. Bull.* **57**, 1810-7 (2012).

30. Andrei, S. R., Sinharoy, P., Bratz, I. N. & Damron, D. S. TRPA1 is functionally co-expressed with TRPV1 in cardiac muscle: co-localization at z-discs, costameres and intercalated discs. *Channels* **10**, 395-409 (2016).

31. Hoebart, C., Rojas-Galvan, N. S., Ciotu, C. I., Aykac, I., Reissig, L. F., Weninger, W. J., Kiss, A., Podesser, B. K., Fischer, M. J. M., Heber, S. No functional TRPA1 in cardiomyocytes.*Acta. Physiol. (Oxf.)* **5**, e13659 (2021).
32. Jordt, S-E., *et al*. Mustard oils and cannabinoids excite sensory nerve fibres through the TRP channel ANKTM1. *Nature*. **427**, 260-5 (2004).
33. Oguri, G. *et al*. Allyl isothiocyanate (AITC) activates nonselective cation currents in human cardiac fibroblasts: possible involvement of TRPA1. *Heliyon*. 7, E05816 (2020).
34. White, E. Mechanosensitive channels: therapeutic targets in the myocardium? *Curr Pharm Des*. **12**, 3645-63 (2006).
35. McNamara, C. R. *et al*. TRPA1 mediates formalin-induced pain. *Proc. Natl. Acad. Sci. U S A.* **104**,13525-30 (2007).
36. Bobkov, Y. V., Corey, E. A, & Ache, B. W. The pore properties of human nociceptor channel TRPA1 evaluated in single channel recordings. *Biochem. Biophys. Acta.* **1808**, 1120-8 (2012).
37. Calaghan, S. C., Belus, A., White, E. Do stretch-induced changes in intracellular calcium modify the electrical activity of cardiac muscle? *Prog. Biophys. Mol. Biol.* **82**, 81-95 (2003).
38. Hartmann, N., *et al*. Antiarrhythmic effects of dantrolene in human diseased cardiomyocytes. *Heart Rhythm* **14**, 412-9 (2017).
39. Smani, T., Dionisio, N., López, J. J., Berna-Erro, A., Rosado, J. A. Cytoskeletal and scaffolding proteins as structural and functional determinants of TRP channels. *Biochim. Biophys. Acta.* **1838**, 658-64 (2014).
40. Schiff, P. B., Fant, J., Horwitz, S. B. Promotion of microtubule assembly in vitro by taxol. *Nature* **277**, 665-7 (1979).

41. Parker, K. K., Taylor, L. K., Atkinson, J. B., Hansen, D. E., Wikswo, J. P. The effects of tubulin-binding agents on stretch-induced ventricular arrhythmias. *Eur. J. Pharmacol*. **417**, 131-40 (2001).

42. Andrei, S. R. *et al*. TRPA1 ion channel stimulation enhances cardiomyocyte contractile function via a CaMKII-dependent pathway. *Channels* **11**, 587-603 (2017).

43. Landstrom, A. P., Dobrev D. & Wehrens, X. H. T. Calcium signaling and cardiac arrhythmias. *Circ. Res.* **120**, 1969-93 (2017).

44. Zurborg, S., Yurgionas, B., Jira, J. A., Caspani, O. & Heppenstall, P. A. Direct activation of the ion channel TRPA1 by Ca^{2+}. *Nat. Neurosci.* **10**, 277-9 (2007).

45. Wang, Y. Y., Chang R. B., Waters, H. N., McKemy, D. D. & Liman, E. R. The nociceptor ion channel TRPA1 is potentiated and inactivated by permeating calcium ions. *J. Biol. Chem.* **21**, 32691-32703 (2008).

46. Andersson, D. A., Gentry, C., Moss, S. & Bevan, S. Transient receptor potential A1 is a sensory receptor for multiple products of oxidative stress. *J. Neurosci.* **28**, 2485-94 (2008).

FIGURES

Figure 1 | Dissociation of repolarisation-relaxation coupling in isolated left ventricular myocytes by activation of ATP-sensitive potassium channels with pinacidil. a, Schematic of the single-excitation/dual-emission fluorescence imaging approach, utilising a single camera-image splitter system. **b,** Representative trace of an action potential (AP, blue) and calcium transient (CaT, red) simultaneously recorded by fluorescence imaging in a rabbit isolated left ventricular myocyte before (left) and after (right) 5 min of pinacidil exposure. The associated vulnerable periods (VP_{RRC}, defined as the period during which myocytes start to become re-excitable while cytosolic calcium (Ca^{2+}) remains elevated, and calculated as the difference between 80% recovery of cytosolic Ca^{2+} to diastolic levels [$CaTD_{80}$]) and 50% recovery of membrane potential [APD_{50}], are shown in green. ECC, excitation-contraction coupling time. **c,** APD_{50} (blue), $CaTD_{80}$ (red), and **d**, VP_{RRC} (green) during 10 min of normal Tyrode (NT, solid) or pinacidil (PIN, dashed) superfusion. Differences assessed by one-way ANOVA, with Tukey *post-hoc* tests. *p<0.05 for NT compared to PIN; †p<0.05 for the change over time; $^{\#}p$<0.05 for the change over time of APD_{50} compared to CaTD. Error bars represent standard error of the mean. *N* = rabbits, *n* = cells.

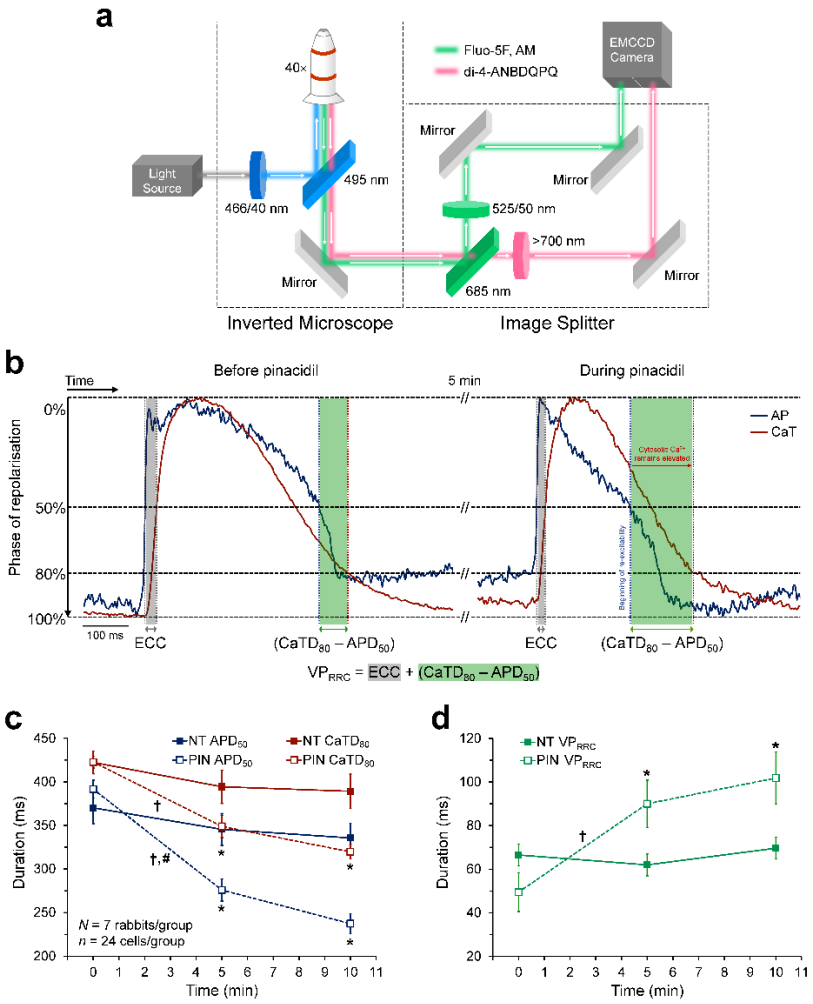

Figure 2 | Arrhythmias elicited by transient stretch of single isolated left ventricular myocytes. a, Representative brightfield image of a rabbit isolated left ventricular myocyte before (left) and during (right) axial stretch using a carbon fibre-based system. Scale bar, 10 µm. **b**, Schematic of the stretch protocol. **c**, Representative measurement of sarcomere length in a cell exposed to pinacidil during 1 Hz pacing (orange dots) and stretched (green segments of trace) in diastole (stretches 1 and 3) or during the VP_{RRC} (stretches 2 and 4) that did not result in an arrhythmia. **d,** Stretch-induced premature contraction (blue segment). **e,** Stretch-induced refractoriness resulting in **e,** a single or **f,** multiple missed beats (red segments). **g,** Stretch-induced sustained arrhythmic activity (red segment) that spontaneously resolved. **h,** Stretch-induced sustained arrhythmic activity (red segment) that was terminated by an additional stretch (second green bar).

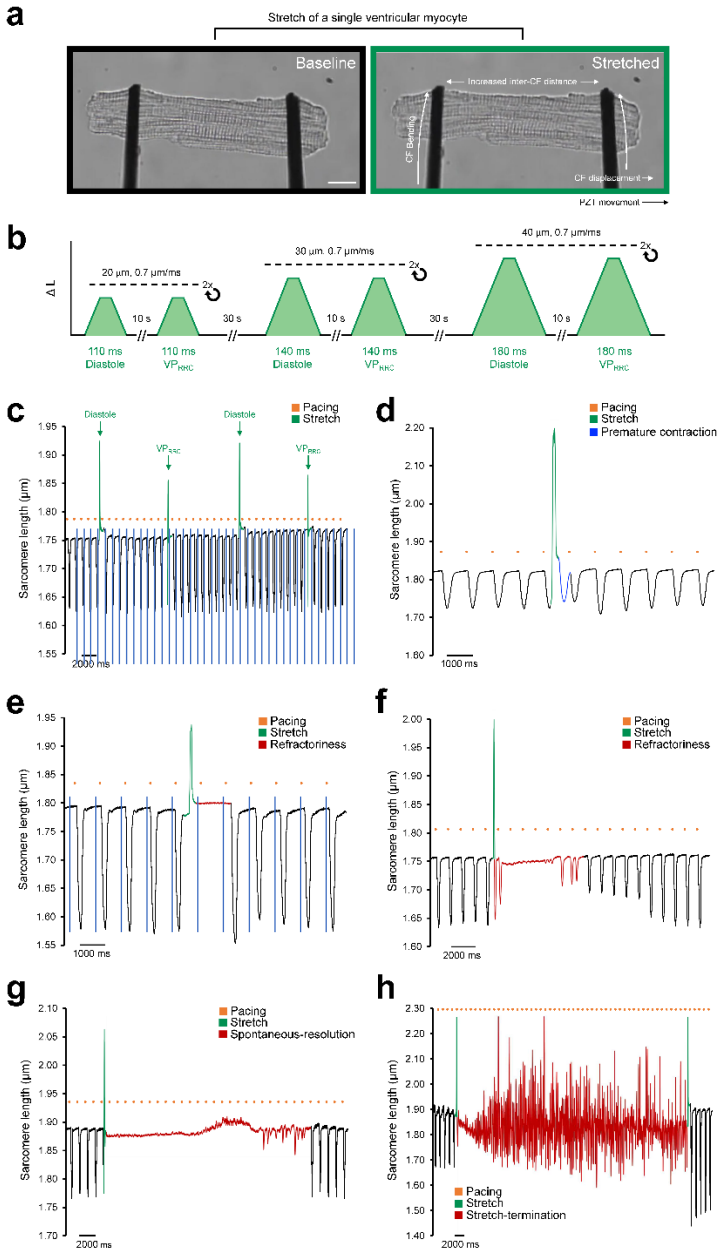

Figure 3 | Effects of pharmacological interventions on mechano-arrhythmogenesis. a, Incidence of premature contractions (blue) and other arrhythmic activity (shades of red) with rapid, transient stretch of rabbit isolated left ventricular myocytes during diastole or the vulnerable period (VP_{RRC}) in cells exposed to one of the following treatments: normal Tyrode (NT); pinacidil (PIN, K_{ATP} channel agonist); PIN + streptomycin (STP, cation non-selective mechano-sensitive channel blocker); PIN + HC-030031 (TRPA1 channel antagonist); PIN + BAPTA (cytosolic calcium, Ca^{2+}, chelator); or PIN + dantrolene (DNT, ryanodine receptor stabiliser). MSC, mechano-sensitive channel. Differences assessed using chi-square contingency tables and Fisher's exact test. **p*<0.05, ***p*<0.01, ****p*<0.001 for Diastole; #*p*<0.05, ##*p*<0.01, ###*p*<0.001 for VP_{RRC}. **b,** Incidence of arrhythmias with stretch during diastole in cells exposed to one of the following treatments: NT; PIN; allyl isothiocyanate (AITC, transient receptor potential kinase ankyrin 1, TRPA1, channel agonist); AITC + HC-030031; AITC + BAPTA; paclitaxel (TAX, microtubule stabiliser); or TAX + HC-030031. Differences assessed using chi-square contingency tables and Fisher's exact test. **p*<0.05, ***p*<0.01, ****p*<0.001. **c,** Percent change in diastolic cytosolic Ca^{2+} concentration after exposure to one of the following treatments: PIN; AITC; PIN + HC-030031; or AITC + HC-030031. Differences assessed using two-tailed, unpaired Student's t-test between groups within PIN or AITC treatment. **p*<0.05. Error bars represent standard error of the mean. *N* = rabbits, *n* = cells, *m* = stretches.

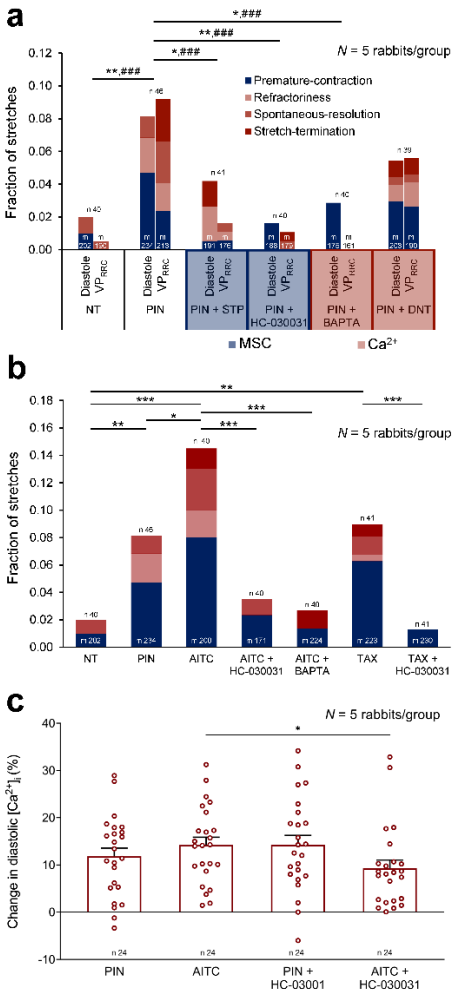

Figure 4 | Role of transient receptor potential kinase ankyrin 1 channels and cytosolic calcium in mechano-arrhythmogenesis. a, Representative trace of voltage (blue) and cytosolic calcium (Ca^{2+}, red) simultaneously recorded by fluorescence imaging in a rabbit isolated left ventricular myocyte exposed to pinacidil (PIN) before and after a rapid, transient stretch (green) that resulted in sustained arrhythmic activity. **Blue inset**, Fluorescence trace (top) and phase plot (bottom) showing changes in voltage preceding Ca^{2+} before stretch. **Red inset**, cytosolic Ca^{2+} oscillations preceding changes in voltage during a sustained arrhythmia after stretch. **b,** Schematic representation of the mechanisms underlying Ca^{2+}-mediated mechano-arrhythmogenesis involving transient receptor potential kinase ankyrin 1 (TRPA1) channels. AITC, Allyl isothiocyanate; NCX, sodium-Ca^{2+} exchanger; PIN, pinacidil; STP, streptomycin.

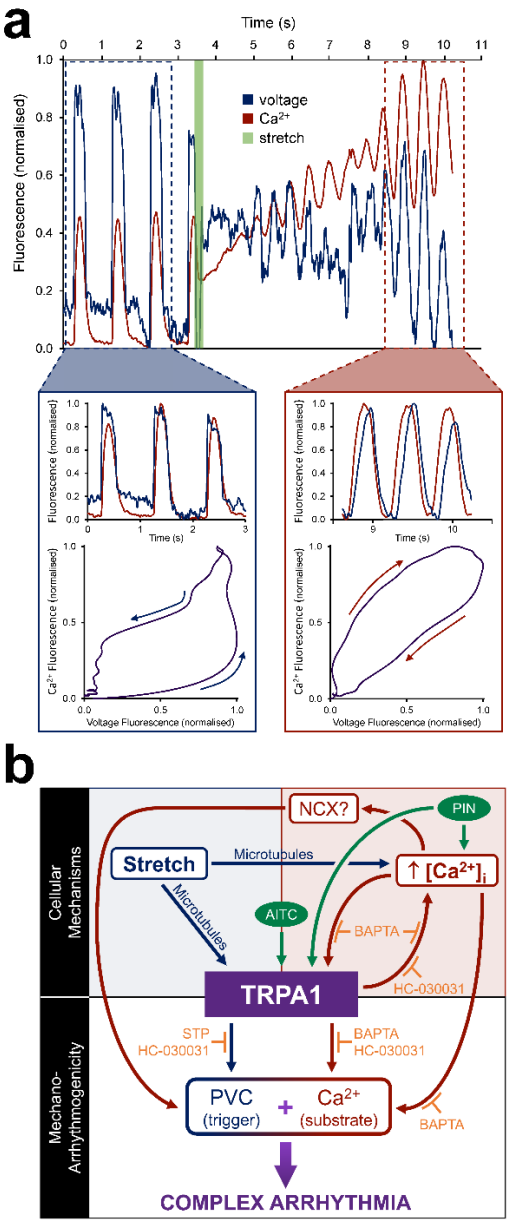

METHODS

Animal model. Experiments involved the use of female New Zealand White rabbits (2.1 ± 0.2 kg, Charles River) - the most relevant small animal model for cardiac arrhythmia research[47] - and were conducted in accordance with the ethical guidelines of the Canadian Council on Animal Care, with protocols approved by the Dalhousie University Committee for Laboratory Animals, or by the local Institutional Animal Care and Use Committee at the University of Freiburg (Regierungspräsidium Freiburg, X-16/10R). Details have been reported following the Minimum Information about a Cardiac Electrophysiology Experiment (MICEE) reporting standard.[48]

Cell isolation. Animals were euthanised by ear vein injection of pentobarbital (140 mg/kg) and heparin (1,500 units/kg, Sigma-Aldrich), followed by rapid excision of the heart, aortic cannulation, and Langendorff perfusion (20 mL/min) with 37°C normal Tyrode (NT) solution (containing, in mM: 120 NaCl, 4.7 KCl, 1 $MgCl_2$, 1.8 $CaCl_2$, 10 glucose, 10 HEPES [Sigma-Aldrich], with pH adjusted to 7.40 ± 0.05 with NaOH and an osmolality of 300 ± 5 mOsm/L) bubbled with 100% oxygen. After a rest period of 15 min, the perfusate was switched to calcium (Ca^{2+})-free solution (containing, in mM: 117 NaCl, 10 KCl, 1 $MgCl_2$, 10 creatine, 20 taurine, 5 adenosine, 2 L-carnitine, 10 glucose, 10 HEPES [Sigma-Aldrich], with pH adjusted to 7.40 ± 0.05 with NaOH and an osmolality of 300 ± 5 mOsm/L) with the addition of 0.018 mM EGTA (Sigma-Aldrich) for 5 min. The perfusate was then switched to digestion solution, comprised of Ca^{2+}-free solution with the addition of 200 U/mL Collagenase II (Worthington Biochemical Corporation), 0.06 mg/mL Protease XIV (from *Streptomyces griseus*, Sigma Aldrich), and 100 μM $CaCl_2$ for 5 min, at which point the perfusion rate was reduced to 15 mL/min until the heart became flaccid and jelly-like (~10-12 min). The left ventricular free wall was removed and placed into 50 mL of stop solution comprised of Ca^{2+}-free solution with the addition of 0.5 % bovine serum albumin

(Sigma Aldrich) and 100 μM $CaCl_2$. The tissue was agitated, the solution filtered through a 300 μm nylon mesh, the tissue returned to fresh stop solution and re-agitated, and the solution filtered. The cell-containing filtered solution was divided into 2 mL microcentrifuge tubes and maintained at room temperature.

Carbon fibre method. Cells were stretched by the carbon fibre method, adapted from previous work.[19] Briefly, a pair of carbon fibres (12-14 μm in diameter, gift of Prof. Peter Kohl, Institute for Experimental Cardiovascular Medicine, University Heart Center Freiburg / Bad Krozingen) were mounted with cyanoacrylate adhesive in borosilicate glass capillaries pulled from glass tubes (1.12 mm inner / 2 mm outer diameter, World Precision Instruments) and bent at 30° 1.2 mm from the end to allow near-parallel alignment of the fibres with the bottom of the experimental chamber. The left and right carbon fibre were trimmed to a length of 1.2 mm and 0.6 mm from the end of the glass capillary, respectively, so that one fibre was relatively compliant and the other relatively stiff. Each carbon fibre was mounted in a microelectrode holder (MEH820, World Precision Instruments) coupled to a three-axis water hydraulic micromanipulator (MHW-103, Narishige) and mounted on a linear piezo-electric translator (PZT, P-621.1CD, Physik Instrumente). The carbon fibre position was controlled by a piezo amplifier / servo controller (E-665.CR, Physik Instrumente) driven by a voltage signal generated from a DAQ device (USB-6361; National Instruments) dictated by custom-written routines in LabVIEW (National Instruments). Carbon fibre stiffness was calculated by pressing a fibre against a force transducer system (406A, Aurora Scientific), measuring the force for given displacements of the PZT, and fitting the data by linear regression to the formula: stiffness = force / PZT displacement. This allowed measurement of force applied during cell stretch by measuring carbon fibre bending through monitoring PZT and fibre tip positions (described below) and applying the formula: force = stiffness × (change in distance

between carbon fibre tips - change in distance between PZTs). Force was then converted to stress by dividing by the unstretched cross-sectional area (CSA), determined by assuming that the cross section is an ellipse with CSA = $\pi \times$ (width/2) $\times$ (thickness/2) and thickness = width/3.

Single cell stretch. Before use, half of the supernatant from the cell-containing microcentrifuge tube was removed and replaced by room temperature NT for 10 min (so that cells were exposed to 50% normal Ca^{2+}), after which all of the supernatant was removed and replaced by NT. A small drop of solution was added to an imaging chamber (RC-27NE2, Warner Instruments) containing 1 mL of NT maintained at 35°C by a temperature controller (TC-344C, Warner Instruments) and mounted on an inverted fluorescence microscope (IX-73, Olympus) with a 40× objective (UPLFLN40X, Olympus). The surface of the coverslip on the bottom of the chamber was coated with poly-2-hydroxyethyl methacrylate (poly-HEMA, Sigma-Aldrich) to prevent cell adhesion. Once the cells had settled, 1 Hz bipolar electrical field stimulation (SIU-102, Warner Instruments) was commenced and normally contracting rod-shaped myocytes with clear striations and well-defined membranes with no signs of blebbing were randomly selected. Electrical stimulation was stopped, and the carbon fibres were positioned at either end of the long axis of a cell and gently lowered onto the cell surface using the hydraulic micromanipulators. Adhesion of the cell to the fibres was confirmed by raising the cell off the coverslip. Once cell attachment was established, electrical stimulation was recommenced, and cells contracted against the carbon fibres for ~1-2 min to improve electrostatic interactions responsible for adhesion. Cells were then superfused at 2.1 mL/min through an inline heater (SF-28, Warner Instruments) with either NT- or pinacidil-containing solution (to activate ATP-sensitive potassium, K_{ATP}, channels) for 5 min. To approximate stretch of ischaemically weakened myocardium during acute regional ischaemia,[49-53] transient stretch (20 μm PZT displacement applied and removed at a rate of 0.7 μm/ms), was

applied (Fig. 2a) during mid-diastole (600 ms delay after an electrical stimulus), followed by a 10 s wait and then stretch during the vulnerable period (VP_{RRC}; 150 ms delay, so that a majority of stretches – whose duration increased with greater PZT displacement – would occur over the entire VP_{RRC}, based on the average VP_{RRC} timing measured by simultaneous voltage-Ca^{2+} imaging, described below), which after another 10 s wait was repeated. This protocol was duplicated at increasing magnitudes of PZT displacement (30 and 40 μm, to generate a range of stretch-induced changes in sarcomere length within a cell), with 30 s between repetitions, for a total of 12 stretches (Fig. 2b).

Assessment of stretch effects. Throughout the protocol, sarcomere length and PZT and carbon fibre tip positions were monitored and recorded at 240 Hz (Myocyte Contractility Recording System, IonOptix). From this, cellular contractile function (diastolic sarcomere length, maximal rate, and percent sarcomere shortening) and characteristics of cell stretch (percent sarcomere stretch, stretched sarcomere length, and maximal applied stress) were measured. Arrhythmic activity was assessed from sarcomere length measurements, which revealed stretch-induced premature contractions (defined as 1 or 2 unstimulated contractions after stretch) or other arrhythmic activity (including refractoriness, resulting in a single or multiple missed beats, or sustained activity that either spontaneously resolved or was terminated by an additional stretch). Examples of each type of stretch-induced arrhythmias is provide in Fig. 2. When a sustained arrhythmia occurred, the next stretch was delayed by the appropriate amount after it resolved (either 10 or 30 s). Any stretch that resulted in slippage of the carbon fibre, or a sustained arrhythmia that did not spontaneously resolve or could not be terminated by a maximum of 2 stretches was excluded (< 1% of all cells), as cell damage could not be excluded as a cause.

Pharmacological interventions. Pharmacologic agents dissolved in distilled water, dimethyl sulfoxide (DMSO), or ethanol as appropriate, were added to the perfusate and continuously perfused for 5 min before cell stretch. Agents included: BAPTA-AM (1 μM, to buffer cytosolic Ca^{2+}, with the concentration determined in preliminary experiments by titrating to a value that caused a ~10% decrease in percent sarcomere shortening during contraction, Abcam), dantrolene (1 μM, to stabilise ryanodine receptors, Abcam), streptomycin (50 μM, to non-specifically block mechano-sensitive channels, Sigma-Aldrich), HC-030031 (10 μM, to block transient receptor potential ankyrin 1, TRPA1, channels, Abcam), allyl isothiocyanate (AITC, 10 μM, to activate TRPA1 channels, Sigma-Aldrich), and paclitaxel (10 μM, to increase the polymerisation and stabilisation of microtubules, Abcam). For BAPTA-AM, HC-030031, and paclitaxel, cells were incubated for 20, 30, or 90 min respectively, after introduction to NT but prior to superfusion.

Dual parametric voltage-Ca^{2+} fluorescence imaging. The Ca^{2+}-sensitive dye Fluo-5F, AM (5 μM, ThermoFisher Scientific) and Pluronic F-127 (0.02 %, Biotium) dissolved in DMSO were added to the cell-containing microcentrifuge tube during cellular suspension in the 50% Ca^{2+} solution and the cells incubated in the dark for 20 min. The supernatant was then replaced with fresh NT, the voltage-sensitive dye di-4-ANBDQPQ (20 μM, University of Connecticut Health Centre) dissolved in ethanol was added to the tube and the cells were incubated in the dark for 14 min. The supernatant was again replaced with fresh NT, probenecid (1 mM, Sigma-Aldrich) was added to the tube, and the cells were maintained in the dark at room temperature. When ready for imaging, the solution containing dye-loaded cells was gently agitated with a transfer pipette and a small drop of solution was added to 1 mL of NT in the imaging chamber. Carbon fibres were adhered to a cell as described above (carbon fibres reduced motion artefact associated with cell movement in the vertical plane during contraction, allowing measurements to be made without an

excitation-contraction uncoupler). Fluorescence was excited by a mercury lamp (U-HGLGPS, Olympus) passed through a 466/40 nm bandpass filter (FF01-466/40, Semrock) and reflected onto the sample by a 495 nm dichroic mirror (FF495-Di03, Semrock). For simultaneous measurement of trans-membrane voltage and cytosolic Ca^{2+}, each fluorescent signal was projected onto one-half of a 128 × 128-pixel, 16-bit electron-multiplying charge-coupled device (EMCCD) camera sensor (iXon3, Andor Technology) using an emission image splitter (Optosplit II; Cairn Research) and recorded at 500 fps with 2 ms exposure time and maximum electron-multiplying gain. The two signals were split with a 685 nm dichroic mirror (FF685-Di02, Semrock) and Fluo-5F emission was collected with a 525/50 nm bandpass filter (FF03-525/50, Semrock) and di-4-ANBDQPQ emission with a 700 nm long-pass filter (HQ700lp; Chroma Technology). A schematic of the imaging setup is in Fig. 1a.

Analysis of voltage-Ca^{2+} signals was performed using custom routines in Matlab (R2018a, MathWorks). Fluorescence for each signal was averaged over the entire cell, a temporal filter (50 Hz low-pass Butterworth) was applied, and bleaching was eliminated by fitting the resulting signal with a second-order polynomial and subtracting the result. From the corrected signals, time to 50% or 80% recovery of the action potential (action potential duration, APD_{50} or APD_{80}) or the Ca^{2+} transient (Ca^{2+} transient duration, $CaTD_{50}$ or $CaTD_{80}$) were averaged over 3 consecutive cardiac cycles. The VP_{RRC} was calculated as the difference between $CaTD_{80}$ and APD_{50}, plus the difference between the timing of the action potential and Ca^{2+} transient upstrokes (excitation-contraction coupling time, ECC, see Fig. 1a): $VP_{RRC} = ECC + (CaTD_{80} - APD_{50})$.

Ratiometric cytosolic Ca^{2+} fluorescence imaging. Imaging of cytosolic Ca^{2+} levels was performed using the ratiometric Ca^{2+}-sensitive dye Fura Red, AM (K_d = 400 nM, AAT Bioquest). Cells were incubated in the dark for 20 min with 5 μM of the dye, 0.02 % Pluronic F-127, and 1

mM probenecid dissolved in DMSO. Fluorescence was excited by alternating light pulses from two white light-emitting diodes (CFT-90-W; Luminus Devices), one with a 420/10 nm bandpass filter (FF01-420/10, Semrock) and the other with a 531/22 nm bandpass filter (FF02-531/22, Semrock), which were combined into the microscope excitation light path with a 455 nm dichroic mirror (AT455dc, Chroma Technology) and reflected onto the sample by a 562 nm dichroic mirror (T562lpxr, Chroma Technology). Fluorescence was measured through a 632/60 nm bandpass filter (AT635/60m, Chroma Technology) with the EMCCD camera at 500 fps with 2 ms exposure time and maximum electron-multiplying gain. Light pulses and camera frame acquisition were synchronised with a custom control box (provided by Dr. Ilija Uzelac, Georgia Institute of Technology) so that alternating frames corresponded to the signal generated by each of the two excitation wavelengths.[54]

Analysis of cytosolic Ca^{2+} was performed using custom routines in Matlab. Fluorescence was averaged over the entire cell and a temporal filter (50 Hz low-pass Butterworth) was applied. The two Ca^{2+} signals were separated, and the ratio of the signals was calculated. Any remaining bleaching was eliminated by fitting the resulting signal with a second-order polynomial and subtracting the result. From the corrected signals, the minimum value for each cardiac cycle (representing a relative measurement of diastolic Ca^{2+} concentration) was measured and averaged over 3 consecutive cardiac cycles.

Cell immunofluorescence. Coverslips (22 mm round; VWR) were coated with laminin (100 µg/mL from Engelbreth-Holm-Swarm murine sarcoma basement membrane diluted in PBS, Sigma-Aldrich) and stored in a 12-well plate (VWR). Isolated myocytes in NT were added to each well and maintained at room temperature for 3 hours to seed. In half of the wells, paclitaxel (10 µM) was added after the first 90 minutes. Cells were then fixed by removing the NT and

submerging the cover slips in ice cold methanol and incubating for 7 minutes at -20ºC. Methanol was removed and cover slips were rinsed 5 times with phosphate buffered saline (PBS, Sigma-Aldrich) to remove excess methanol. Cover slips were stored in PBS until staining.

For staining, coverslips were bathed in blocking solution (5% BSA in PBS, Sigma-Aldrich) at room temperature. After 1 hour, plates were transferred to 100 µL of a primary antibody storage solution (5% BSA in PBS) in a custom-built humidity chamber (glass petri dish lined with a PBS-soaked Kimwipe and sealed with Parafilm). Diluted primary antibody (100 µL of 1:200 rat anti-rabbit α-tubulin, Clone YL1/2, Invitrogen) was placed on the parafilm and the coverslip was mounted cell-side down and incubated at 4ºC for 1 hour. Coverslips were subsequently washed in quadruplicate (5 min each) with PBS and diluted secondary antibody (1:500 goat anti-rat IgG Alexa Fluor 488 conjugate, Invitrogen) was applied as above. Following secondary antibody staining, coverslips were mounted to glass slides with mounting medium (ProLong Glass Antifade Mountant with NucBlue Stain, ThermoFisher).

Imaging of the fixed and stained myocytes was performed on an inverted confocal microscope (TCS SP8, Leica) system with a 40× oil, 1.3 NA objective (HC Plan APOCHROMAT CS2, Leica) and Lightning deconvolution software to obtain near super-resolution images. Samples were illuminated with a 488 nm solid state laser at 1.2% intensity and the photomultiplier tube (PMT) detectors were set to collect between 503-577 nm. A 1.5 µm z-stack of 3 images was obtained. Maximum projections of confocal z-sections were generated using Leica LAS X 3D viewer software. Images were then analysed in a blinded fashion using custom software in Fiji (kindly shared by Drs. Matthew Caporizzo and Benjamin Prosser, Department of Physiology, University of Pennsylvania Perelman School of Medicine, Philadelphia, USA) to determine microtubule density, calculated as the fraction of cell area.[55] Briefly, cells were manually traced and a threshold

for microtubule positive pixels was determined from a background region within the cell with no visible microtubule fluorescence. This was used to generate a binary image of the cell to calculate the microtubule positive fraction of the total cell area.

Tissue western blotting. Boiled samples of left ventricular free wall (20 μg) were separated (4% stacking gel) and resolved *via* 7.5% sodium dodecyl sulfate-polyacrylamide gel electrophoresis (Mini-PROTEAN SDS-PAGE, BioRad). Samples were loaded alongside 10 μL protein ladder (Precision Plus Protein Standards Kaleidoscope ladder, BioRad). Self-cast gels (Mini-PROTEAN, BioRad) were run on ice at 90 V for 30 min and then at 120 V until the dye front migrated to the bottom edge of the gel on ice in 1X Tris/Glycine/SDS electrophoresis buffer (BioRad). Samples were wet-transferred to nitrocellulose (0.2 μm, BioRad) at 100 V for 1.5 hrs buried in ice. Membranes were briefly rinsed in double-distilled water and equal protein transfer was confirmed by incubating the membranes in stain (Pierce Reversible Memcode Stain, Thermo Scientific) for 5 min. The stained blot was labelled and imaged (ChemiDoc MP Imaging System, BioRad) before removing the stain (Pierce Stain Eraser, Thermo Scientific). Membranes were then blocked in 5% skim-milk in 1X Tris-Buffered-Saline-Tween 20 (TBS-T, Sigma-Aldrich) for 60 min. Membranes were subsequently incubated overnight at 4ºC with primary antibodies (1:2000 monoclonal anti-TRPA1 antibody produced in mouse, Sigma-Aldrich, and 1:3000 MF20 anti-myosin heavy chain, Hybridoma Bank), diluted in 1% skim-milk in TBS-T with sodium azide. Next, blots were incubated with secondary antibody (1:4000 horseradish peroxidase HRP-conjugated anti-mouse, Jackson Labs) for 1 hour in 5% skim-milk at room temperature. Immunoreactivity was then measured (Clarity Western Enhanced Chemiluminescence Substrate, with a ChemiDoc MP Imaging System, BioRad). Membranes were stripped by incubation in 25 mL 0.5 M Tris-HCl/SDS buffer supplemented with 125 μL 2-mercaptoethanol (Sigma-Aldrich) for 1 hour and re-probed.

Patch-clamp current recordings. Cells for patch clamp experiments were isolated from acute ventricular slices according to a previously published protocol.[56] Briefly, animals were anaesthetised by intramuscular injection of esketamine hydrochloride (0.5 mL/kg) and 2% xylazine hydrochloride (0.2 mL/kg). Under sedation, an anaesthetic mixture of sodium-heparin (1,000 units/mL) and esketamine hydrochloride (25 mg/mL) were injected intravenously. Euthanasia was induced by intravenous injection of sodium-thiopental (25 mg/mL) until apnoea. The heart was then excised, cannulated, and Langendorff perfused (20 mL/min) for 2 min with 37°C modified NT solution (containing, in mM: 137 NaCl, 4 KCl, 10 $MgCl_2$, 1.8 $CaCl_2$, 10 glucose, 10 HEPES, 10 creatine, 20 taurine, 5 adenosine, 2 L-carnitine; with pH adjusted to 7.30 ± 0.05 with NaOH) bubbled with 100% oxygen, followed by 2 min with 37°C cutting solution (containing, in mM: 138 NaCl, 5.4 KCl, 0.33 NaH_2PO_4; 2.0 $MgCl_2$, 0.5 $CaCl_2$, 10 HEPES, 30 2,3-butanedione 2-monoxime (BDM); with pH adjusted to 7.30 ± 0.05 with NaOH) bubbled with 100% oxygen. The left ventricular free wall was cut into approximately 0.8 mm x 0.8 mm chunks, embedded in 4% low melting point agarose, dissolved in cutting solution, and cut into 300 µm thick slices using a vibrating microtome (7000 smz-2, Campden Instruments Ltd) with stainless-steel blades (7550-1-SS, Campden Instruments Ltd) at 4°C, a frequency of 60 Hz, an amplitude of 1.5 mm, a velocity of 0.05 mm/s, and Z-deflection calibrated to values below 1 µm. Slices were stored at 4°C in cutting solution until digestion.

Slices were digested at 37°C in petri dishes (Ø 35 mm) placed on a heated orbital shaker (50-65 revolutions per min). Slices were washed three times with digestion solution (containing, in mM: 100 NaCl, 15 KCl, 2.5 KH_2PO_4, 2 $MgCl_2$, 10 glucose, 10 HEPES, 20 taurine, 20 L-glutamic acid monopotassium salt, 30 BDM; with 2 mg/mL bovine serum albumin and pH adjusted to 7.30 ± 0.05 with NaOH), including a 1 min incubation for each wash. Slices were then digested for 12

min by including protease type XXIV (0.5 mg/mL; Sigma-Aldrich), followed by three more washes. Digestion was continued by adding 200 μL of Liberase™ TL Research Grade (0.25 mg/mL; Hoffmann-La Roche) per 2 mL of digestion solution, supplemented with 5 μM $CaCl_2$. When slices started to appear accordion-like (~25-50 min), they were washed three times with digestion solution containing 10 mg/mL bovine serum albumin and mechanically dissociated using forceps and gentle pipetting with Pasteur pipettes. Ca^{2+} concentration was increased in a stepwise fashion every 5 min (5 μM, 12 μM, 20 μM, 42 μM, 84 μM, 162 μM, 266 μM, 466 μM, 827 μM, and 1 mM), during which time BDM was gradually decreased to a final concentration of 13 mM. The tissue was filtered through a 1 mm nylon mesh and allowed to settle in a conical centrifuge tube for 15-20 min. The supernatant was removed by washing with modified NT. Quality of the preparation was assessed by the percentage of rod-shaped cells, the response to electrical pacing, and the resting sarcomere length.

Sarcolemmal ion channel activity was recorded at room temperature (21 ± 2°C) using the patch-clamp technique with voltage clamped at +40 mV. Fire-polished soda-lime glass capillaries (1.15 ± 0.05 mm inner / 1.55 ± 0.05 mm outer diameter; VITREX Medical A/S) were pulled using a two-stage pipette-puller (PC-10, Narishige) to create the micropipettes required for patch-clamping. Average pipette resistance was 1.36 ± 0.10 MΩ. Recordings were obtained in cell-attached configuration using a patch-clamp amplifier (Axopatch 200B, Axon Instruments) and a digitiser interface (Axon Digidata 1440A, Axon Instruments). Currents were acquired at 20 kHz sampling rate (interval 50 μs), and low-pass filtered at 1 kHz. Currents were analysed with pCLAMP 10.6 software (Axon Instruments). The bath solution contained (in mM): 155 KCl, 3 $MgCl_2$, 5 EGTA, 10 HEPES (Sigma-Aldrich), with pH adjusted to 7.2 ± 0.05 using KOH and an osmolality of 300 ± 5 mOsm/L. The solution was stored at room temperature. Pipette solution for

cell-attached recordings contained (in mM): 150 NaCl, 5 KCl, 10 HEPES, 2 $CaCl_2$ with pH adjusted to 7.4 ± 0.05 using NaOH and an osmolality of 300 ± 5 mOsm/L. The pipette solution also contained 10 mM tetraethylammonium chloride (TEA), 5 mM 4-aminopyridine, and 10 mM glibenclamide to inhibit eventual contaminating potassium channels. These ionic conditions were used previously to describe cation non-selective channels.[57] AITC was added to the bath solution before use and perfused *via* a local perfusion system. Flow rate was adapted by adjusting the height of reservoirs for gravity-fed flow to 1 mL/min. Recordings were analysed in Clampfit 10.6. Average current was calculated over at least 10 s for each condition.

Statistics. Statistics were performed using Prism 9 (GraphPad). Differences in arrhythmia incidence were assessed using chi-square contingency tables and Fisher's exact test. Data was first tested for normality, then differences between group means were assessed by two-tailed, paired or unpaired Student's t-test (for normally distributed data), Wilcoxon matched-pairs (paired) or Mann-Whitney (unpaired) test (for data that was not normally distributed), one-way ANOVA with Tukey *post-hoc* tests (for normally distributed data), or Kruskal-Wallis with Dunn's multiple comparisons test (for data that was not normally distributed), where appropriate. The relevant test is indicated in the figure captions. A p-value of < 0.05 was considered significant. Figures indicate the number of replicates used in each experiment (N = rabbits, n = cells, m = stretches).

Data availability. The datasets generated in the current study are available from the corresponding author upon reasonable request.

Code availability. All custom computer source code used in this study is available from the corresponding author upon reasonable request.

METHODS REFERENCES

47. Clauss, S. *et al*. Animal models of arrhythmia: classic electrophysiology to genetically modified large animals. *Nat. Rev. Cardiol*. **16**, 457-75 (2019).
48. Quinn, T. A. *et al*. Minimum Information about a Cardiac Electrophysiology Experiment (MICEE): standardised reporting for model reproducibility, interoperability, and data sharing. *Prog. Biophys. Mol. Bio.* **107**, 4-10 (2011).
49. Gallagher, K. P., Gerren, R. A., Choy M., Stirling M. C. & Dysko R. C. Subendocardial segment length shortening at lateral margins of ischaemic myocardium in dogs. *Am. J. Physiol*. **253**, H826-37 (1987).
50. Prinzen, F. W., Arts, T., Hoeks, A. P. G. & Reneman, R. S. Discrepancies between myocardial blood flow and fiber shortening in the ischaemic border zone as assessed with video mapping of epicardial deformation. *Pflügers Archiv*. **415**, 220-9 (1989).
51. Sakai, K., Watanabe, K., Millard, R. W. Defining the mechanical border zone: a study in the pig heart. *Am. J. Physiol*. **249**, H88-94 (1985).
52. Theroux, P., Franklin, D., Ross, J., Kemper, W. S. Regional myocardial function during acute coronary artery occlusion and its modification by pharmacologic agents in the dog. *Circ. Res*. **35**, 896-908 (1974).
53. Rodriguez, F. et al. Alterations in transmural strains adjacent to ischemic myocardium during acute midcircumflex occlusion. *J. Thorac. Cardiovasc. Surg*. **129**, 791-803 (2005).
54. Lee, P., Bollensdorff, C., Quinn, T. A., Wuskell, J. P., Loew, L. M. & Kohl, P. Single-sensor system for spatially-resolved, continuous and multi-parametric optical mapping of cardiac tissue. *Heart Rhythm*. **8**, 1482-91 (2011).

55. Chen, C. Y., Caporizzo, M. A., Bedi, K., Vite, A., Bogush, A. I., Robison, P., Heffler, J. G., Salomon, A. K., Kelly, N. A., Babu, A., Morley, M. P., Margulies, K. B., Prosser, B. L. Suppression of detyrosinated microtubules improves cardiomyocyte function in human heart failure. *Nat. Med*. **24**, 1225-33 (2018).

56. Fiegle, D. J., Volk, T., Seidel, T. Isolation of human ventricular cardiomyocytes from vibratome-cut myocardial slices. *J. Vis. Exp.* **159**, e61167 (2020).

57. Peyronnet, R. *et al*. Piezo1-dependent stretch-activated channels are inhibited by Polycystin-2 in renal tubular epithelial cells. *EMBO Rep*. **14**, 1143-8 (2013).

STATEMENTS

Acknowledgements. We thank Gentaro Iribe and Keiko Kaihara for technical assistance with cell stretch and Ilija Uzelac for technical assistance with electronic LED control. Carbon fibres are a gift from Jean-Yves LeGuennec. This work was supported by the Canadian Institutes of Health Research (MOP 342562 to T.A.Q.); by the Natural Sciences and Engineering Research Council of Canada (RGPIN-2016-04879 to T.A.Q.); by the Dalhousie Medical Research Foundation (T.A.Q.); by the Canadian Foundation for Innovation (32962 to T.A.Q.); and by the Heart and Stroke Foundation of Canada through a National New Investigator award (T.A.Q.). R.P. and P.K. are members of the German Research Foundation Collaborative Research Centre 1425 (422681845).

Author contributions. B.A.C. and T.A.Q. designed the study, interpreted the data, and wrote the manuscript; B.A.C. performed and analysed the cell stretch and fluorescence imaging experiments and isolated cells for the immunofluorescence experiments; M.R.S. contributed to experimental design and setup; J.G. isolated cells for the patch-clamp experiments; R.P. performed and analysed the patch-clamp experiments; M.S.C. performed and analysed the Western blotting experiments; and J.J.B. performed and analysed the immunofluorescence experiments. P.K. contributed to the intellectual content of the research and revised the manuscript. All authors read and approved the manuscript.

Author information. The authors declare no competing interests. Correspondence and request for materials should be addressed to T.A.Q. (alex.quinn@dal.ca).

EXTENDED DATA

Extended Data Figure 1 | Mechanical characteristics of cell stretch. a, Percent sarcomere stretch, **b,** stretched sarcomere length, and **c,** maximal applied stress during rapid, transient diastolic stretch of rabbit isolated left ventricular myocytes exposed to normal Tyrode (NT, grey) or pinacidil (PIN, white) with increasing levels of piezo-electric translator (PZT) displacement (20, 30, and 40 μm). Differences assessed by one-way ANOVA, with Tukey *post-hoc* tests for **a** and **b**, and by Kruskal-Wallis test for **c**. **p*< 0.05, ***p*< 0.01, ****p*< 0.001. *N* = rabbits, *n* = cells.

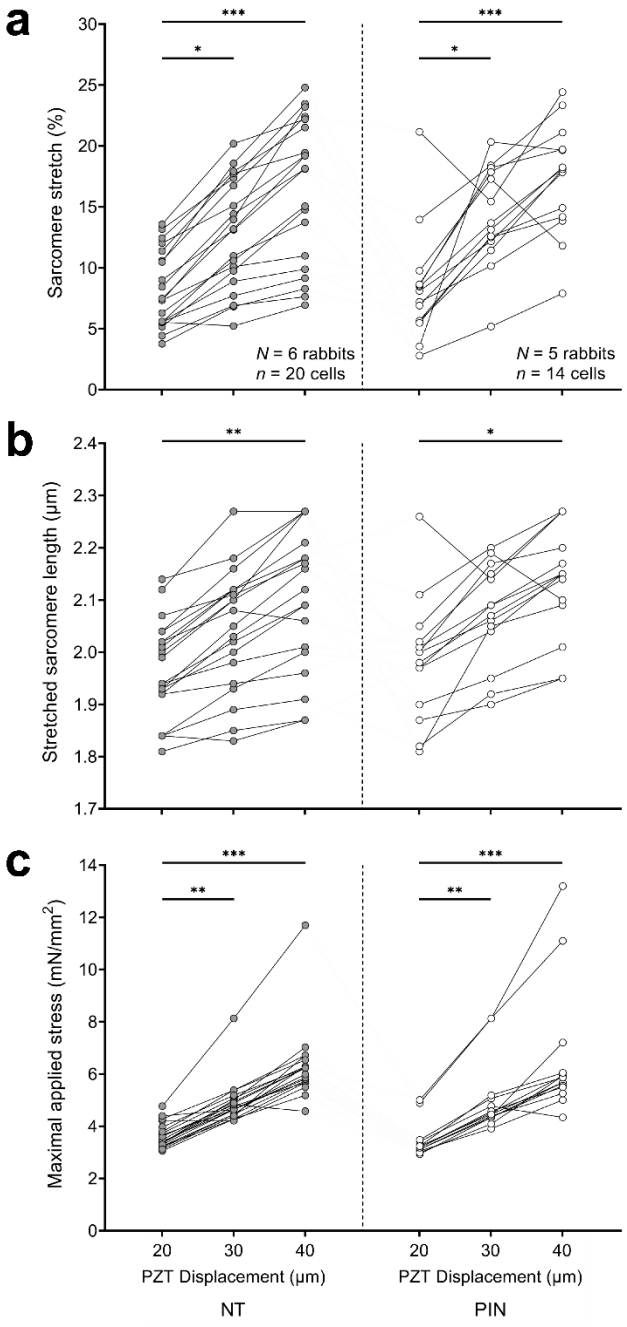

Extended Data Figure 2 | Effect of pharmacological interventions on mechano-arrhythmogenesis in control conditions. Incidence of premature contractions (blue) and other arrhythmic activity (shades of red) with rapid, transient stretch of rabbit isolated left ventricular myocytes during diastole or the vulnerable period (VP_{RRC}) exposed to one of the following treatments: normal Tyrode (NT); NT + streptomycin (STP); NT + HC-030031; NT + BAPTA; or NT + dantrolene (DNT). Ca^{2+}, calcium; MSC, mechano-sensitive channels. Differences assessed using chi-square contingency tables and Fisher's exact test. *N* = rabbits, *n* = cells, *m* = stretches.

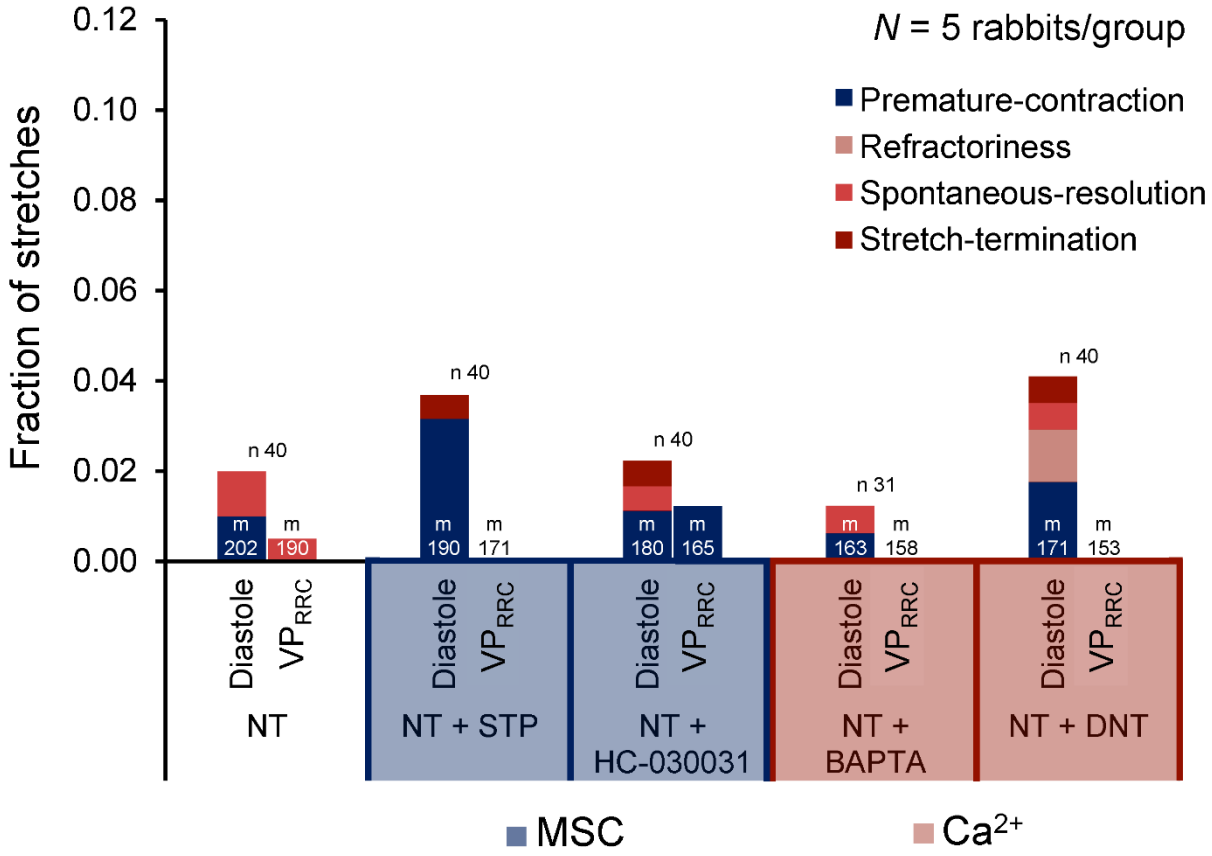

Extended Data Figure 3 | Effect of stretch magnitude on the incidence of mechano-arrhythmogenesis. Incidence of premature contractions (blue) and other arrhythmic activity (shades of red) with rapid, transient stretch at increasing levels of piezo-electric translator (PZT) displacement in rabbit isolated left ventricular myocytes exposed to either normal Tyrode (NT, left) or pinacidil (PIN, right). Differences assessed using chi-square contingency tables and Fisher's exact test. *p< 0.05. N = rabbits, n = cells, m = stretches.

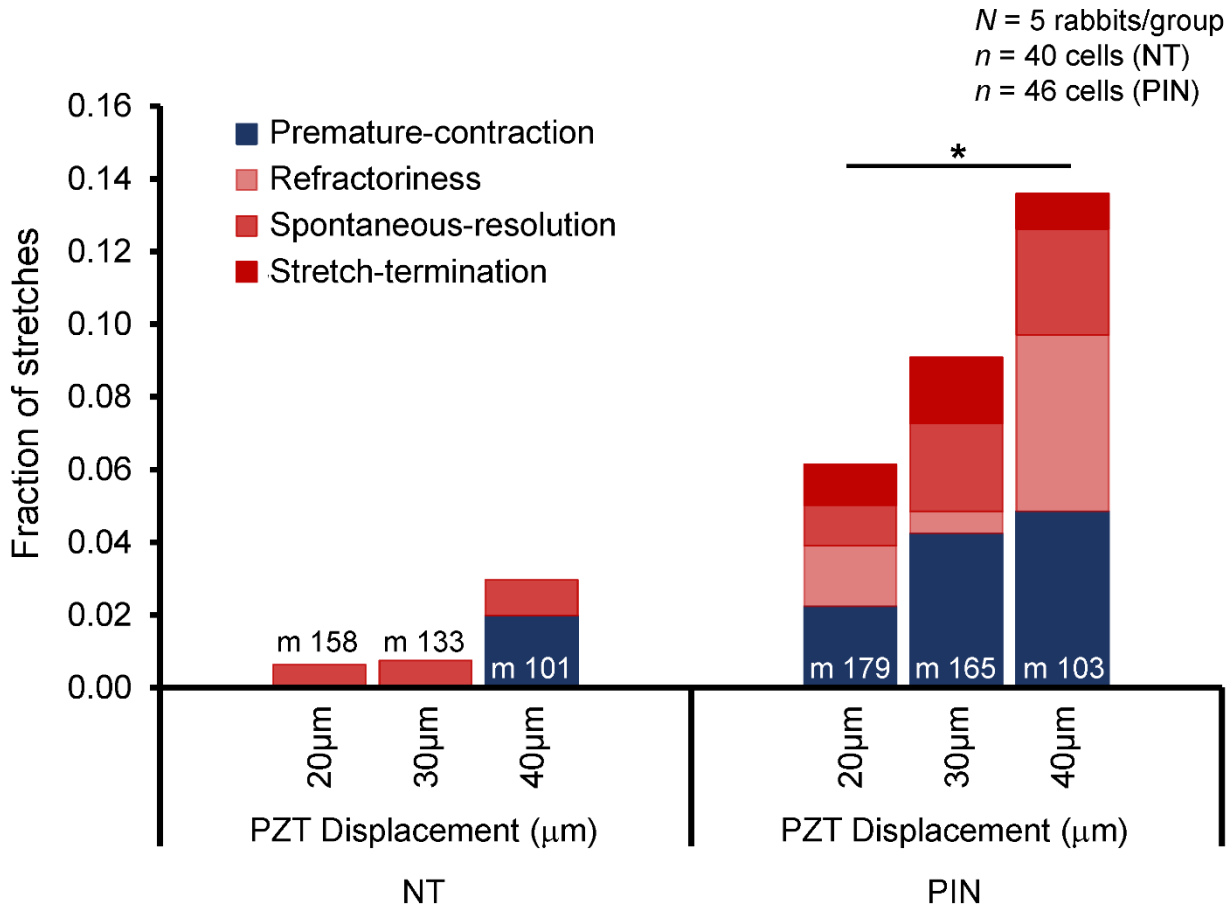

Extended Data Figure 4 | Contractile function before and after stretch. a, Diastolic sarcomere length and **b,** maximal rate and **c,** percent sarcomere shortening during contraction of rabbit isolated left ventricular myocytes exposed to either normal Tyrode (NT, grey) or pinacidil (PIN, white) before (pre-stretch) and after three successive diastolic stretches generated with an increasing level of piezo-electric translator (PZT) displacement. Measurements for each point averaged over 5 contractions. Differences assessed by one-way ANOVA, with Tukey *post-hoc* tests. *$p < 0.05$. N = rabbits, n = cells.

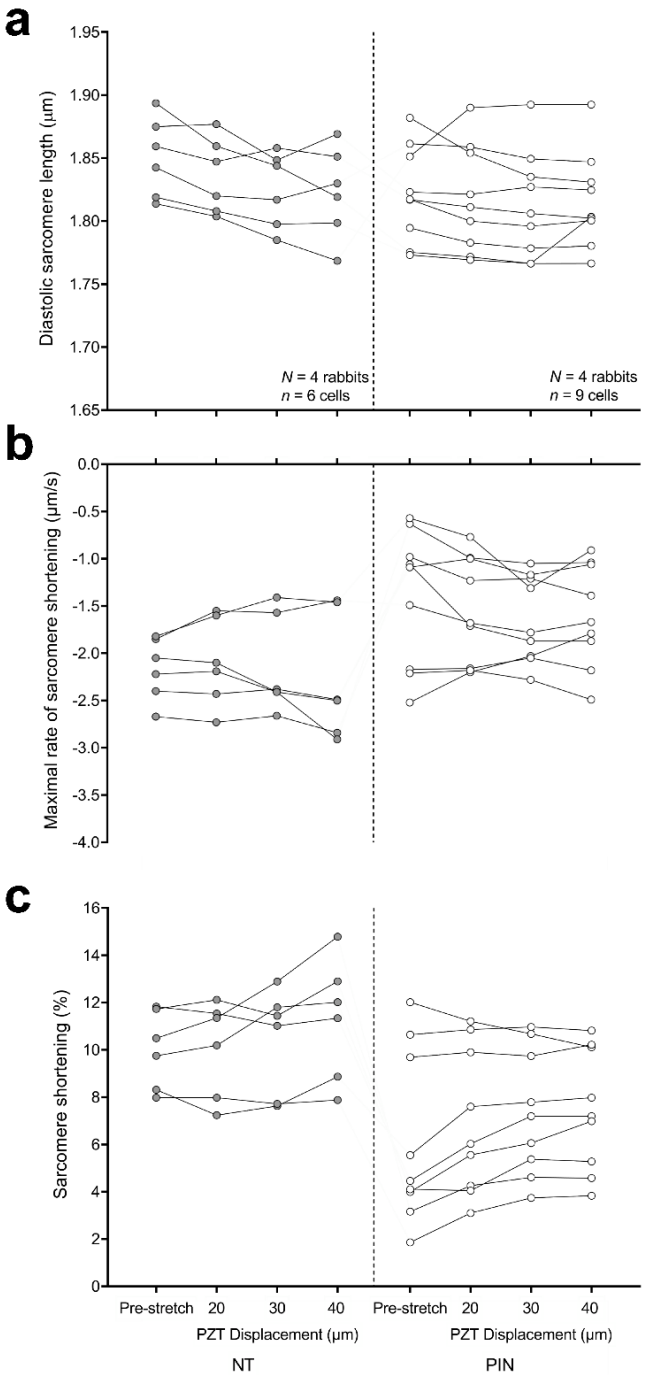

Extended Data Figure 5 | Contractile function after sustained arrhythmic activity. a, Diastolic sarcomere length and **b,** maximal rate and **c,** percent sarcomere shortening during contraction of rabbit isolated left ventricular myocytes exposed to pinacidil before (green) and after (red) termination of stretch-induced sustained arrhythmic activity. Measurements for each point averaged over 5 contractions. Differences assessed using two-tailed, paired Student's t-test. *p<0.05. N = rabbits, n = cells.

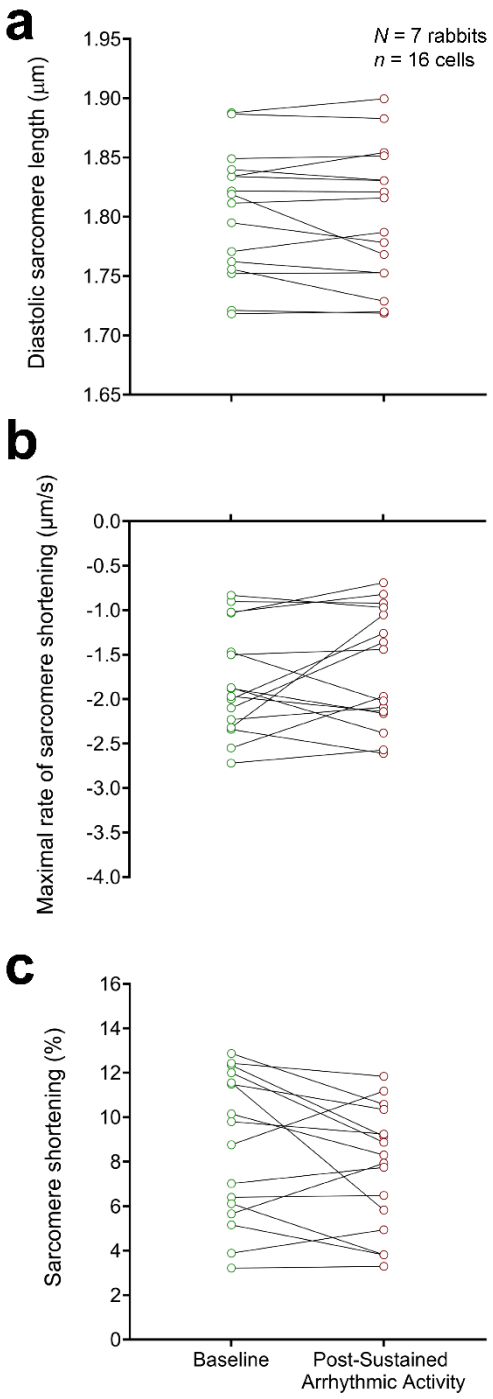

Extended Data Figure 6 | Expression of transient receptor potential ankyrin 1 channels in rabbit left ventricular myocytes. a, Western blot of transient receptor potential ankyrin 1 (TRPA1) and myosin heavy chain (MF20) protein expression in rabbit left ventricular free wall tissue. **b**, Representative recording of channel activation in response to AITC exposure in a cell-attached patch at +40 mV. **Inset**, Detail of channel activation with visible single channel events. **c**, Quantification of either AITC-induced current (left), or current in time-matched controls (right). Differences assessed with two-tailed, paired Student's t-test. $^{**}p<0.01$. Error bars represent standard error of the mean. N = rabbits, n = cells.

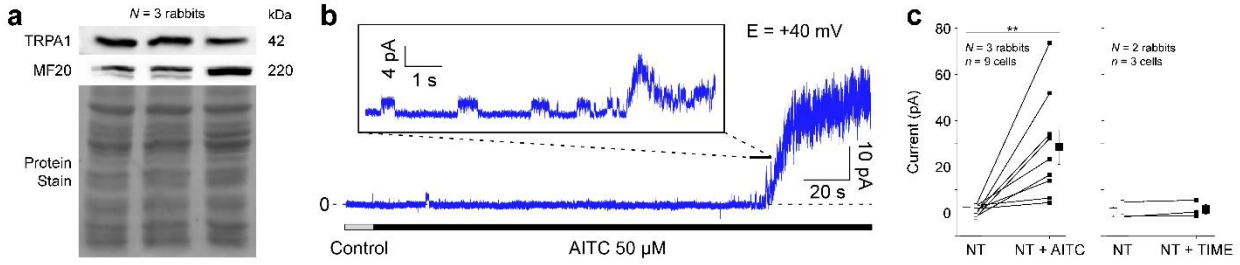

Extended Data Figure 7 | Effect of pharmacological interventions on contractile function in control conditions. a, Diastolic sarcomere length and **b**, maximal rate and **c**, percent sarcomere shortening during contraction of rabbit isolated left ventricular myocytes exposed to one of the following treatments: normal Tyrode (NT); NT + streptomycin (STP); NT + HC-030031; NT + BAPTA; or NT + dantrolene (DNT). Differences assessed by one-way ANOVA, with Tukey *post-hoc* tests for **a** and **b** and by Kruskal-Wallis test for **c**. *$p < 0.05$, ***$p < 0.001$. Error bars represent standard error of the mean. N = rabbits, n = cells.

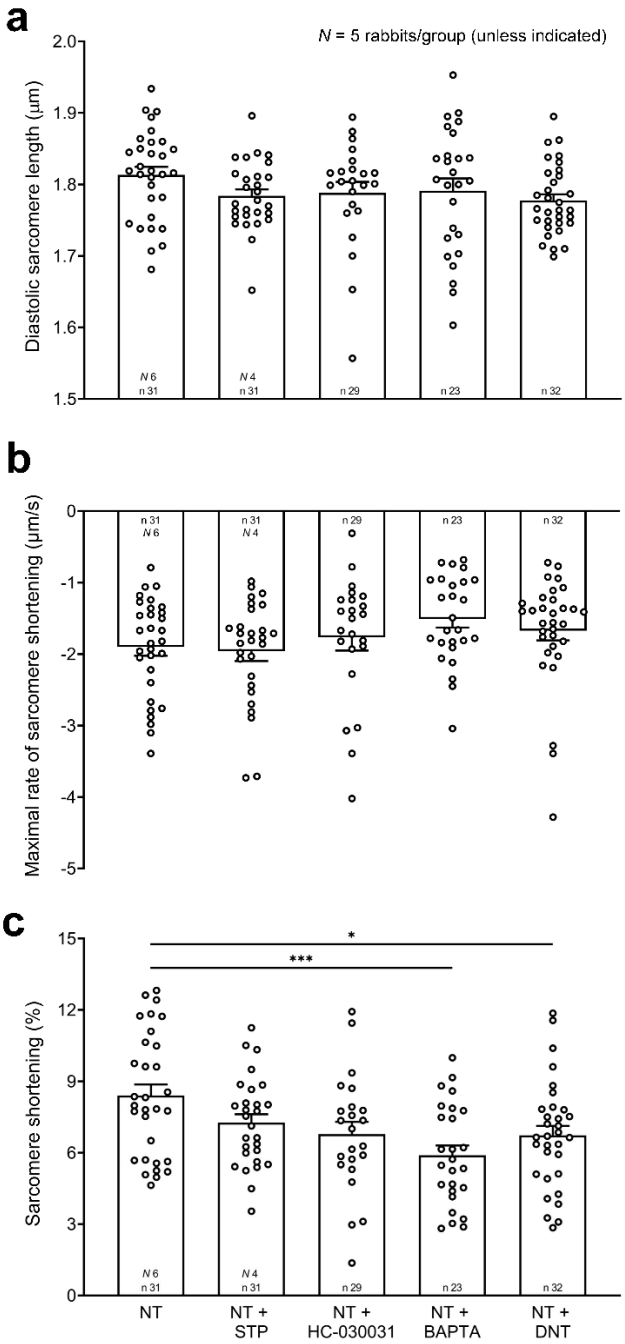

Extended Data Figure 8 | Effect of paclitaxel on microtubule density. Confocal immunofluorescence images of stained microtubules in rabbit isolated left ventricular myocytes either **a,** in control or **b,** following paclitaxel exposure. **c,** Quantification of microtubule density assessed as the microtubule positive fraction of total cell area. Difference assessed with two-tailed, unpaired Student's t-test. *p<0.05. Error bars represent standard error of the mean. N = rabbits.

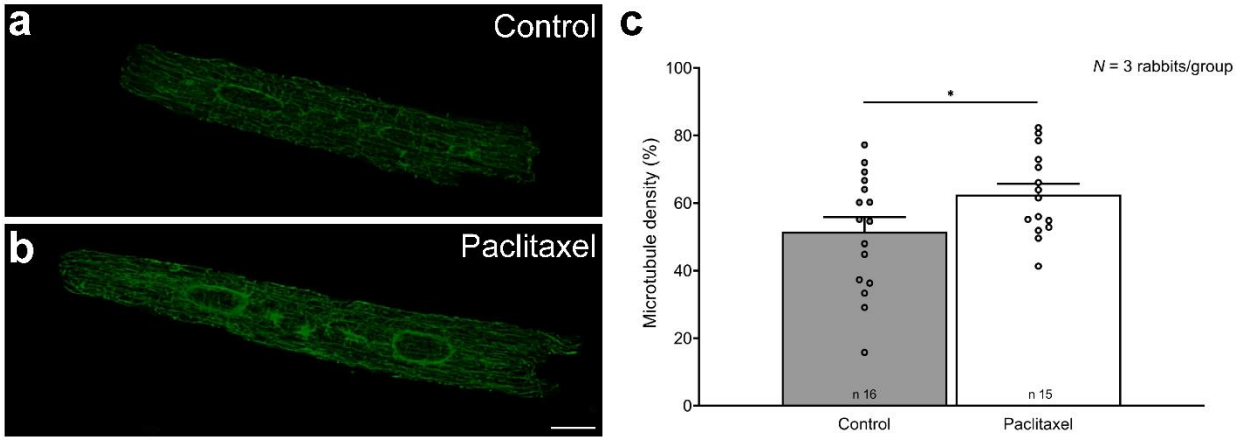

Extended Data Figure 9 | Effect of pinacidil on cellular mechanics. a, Stiffness (represented by the slope of the end-diastolic stress-length relationship, EDSLR, blue) and elastance (represented by the slope of the end-systolic stress-length relationship, ESSLR, red) of rabbit isolated left ventricular myocytes exposed to either normal Tyrode (NT) or pinacidil (PIN). **b,** Calculated stiffness, elastance, and stiffness-sarcomere length (SL) and elastance-SL intercept in cells exposed to either NT (grey) or PIN (white). Differences assessed using two-tailed, unpaired Student's t-test. $^{**}p < 0.01$, $^{***}p < 0.001$. Error bars represent standard error of the mean. N = rabbits, n = cells.

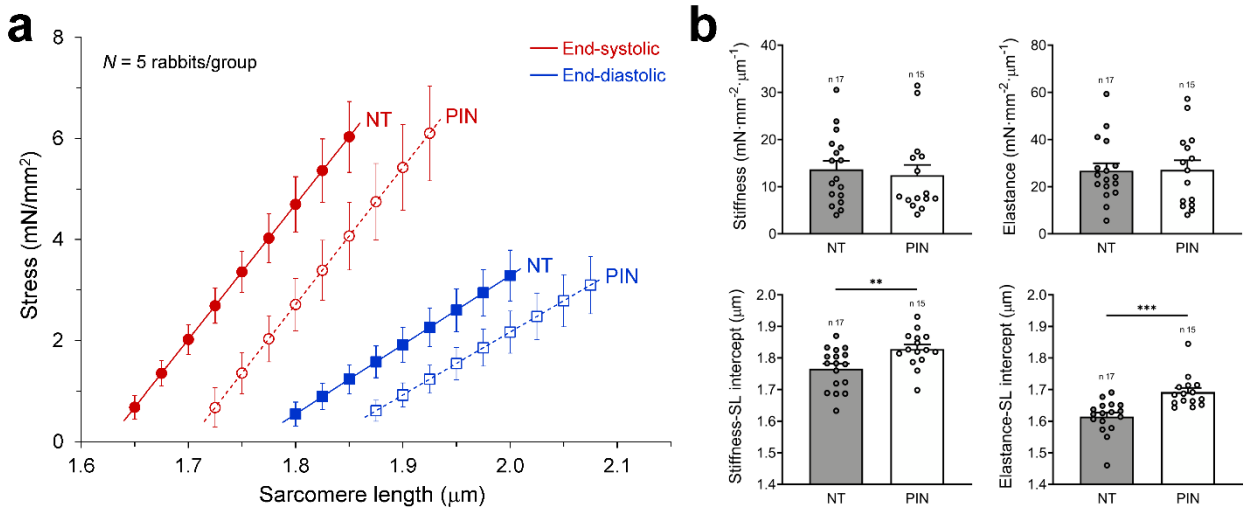

Extended Data Figure 10 | Mechanical characteristics of cell stretch with differing electrophysiological outcomes. a, Maximal applied stress, **b,** percent sarcomere stretch, and **c,** maximal sarcomere length for two consecutive rapid, transient diastolic stretches of pinacidil (PIN)-treated rabbit isolated left ventricular myocytes, for which one stretch caused an arrhythmia (ARR, red) and the other remained in normal paced rhythm (NPR, green). Differences assessed using the Wilcoxon matched-pairs test. *p< 0.05. N = rabbits, n = cells.

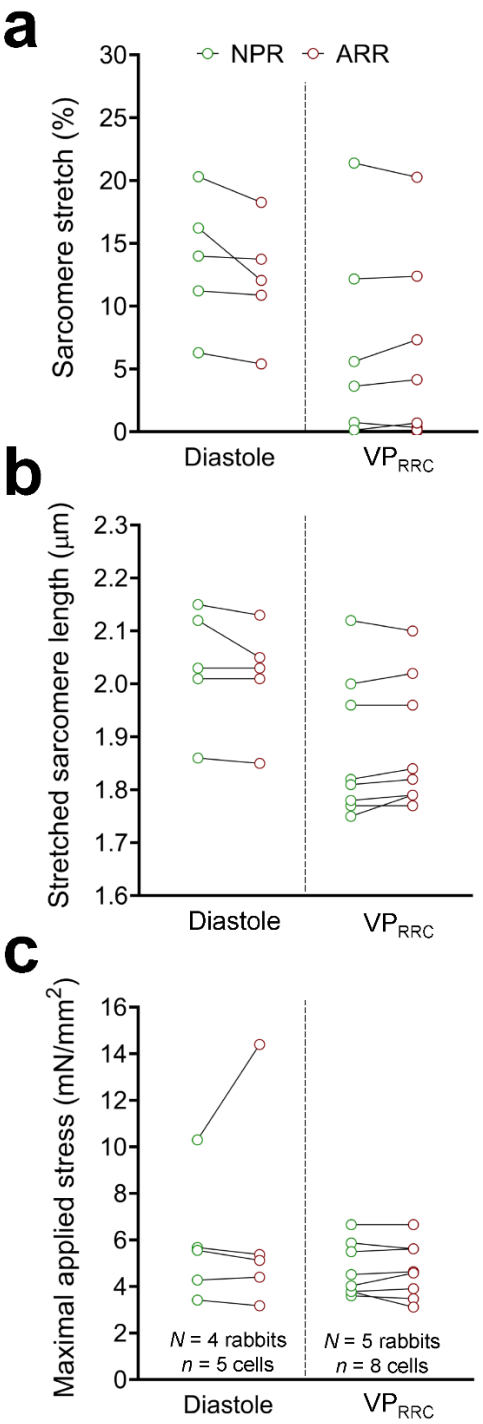

SUPPLEMENTARY INFORMATION

Supplementary Video 1 | Stretch-induced premature contraction. Example of rapid, transient stretch of a rabbit isolated left ventricular myocyte treated with pinacidil, applied using microscopic carbon fibres adhered to either end of the cell, which resulted in a premature contraction. Sarcomere dynamics and carbon fibre positions were simultaneously measured to assess arrhythmic incidence and confirm maintenance of contractile function (representative sarcomere trace shown in Fig. 2d).

Supplementary Video 2 | Stretch-induced refractoriness. Example of rapid, transient stretch of a rabbit isolated left ventricular myocyte treated with pinacidil, applied using microscopic carbon fibres adhered to either end of the cell, which resulted in refractoriness. Sarcomere dynamics and carbon fibre positions were simultaneously measured to assess arrhythmic incidence and confirm maintenance of contractile function (representative sarcomere trace shown in Fig. 2f).

Supplementary Video 3 | Stretch-induced sustained arrythmia with termination by stretch. Example of rapid, transient stretch of a rabbit isolated left ventricular myocyte treated with pinacidil, applied using microscopic carbon fibres adhered to either end of the cell, which resulted in a sustained arrhythmia that was terminated by application of an additional stretch. Sarcomere dynamics and carbon fibre positions were simultaneously measured to assess arrhythmic incidence and confirm maintenance of contractile function (representative sarcomere trace shown in Fig. 2h).

Supplementary Video 4 | Stretch-induced, calcium-driven sustained arrhythmia. Example of simultaneous voltage (blue)-calcium (red) fluorescence imaging in a rabbit isolated ventricular myocyte treated with pinacidil. Rapid, transient stretch during the vulnerable period (green bar) resulted in sustained arrhythmic activity, in which oscillations in cytosolic calcium preceded changes in voltage, indicating calcium-driven activity (see inset and Fig. 4a).